Demixing of homogeneous binary lipid membranes induced by protein inclusions

Piotr Nowakowski
Max-Planck-Institut für Intelligente Systeme Stuttgart, Heisenbergstr. 3, 70569 Stuttgart, Germany;
Institut für Theoretische Physik IV, Universität Stuttgart, Pfaffenwaldring 57, 70569 Stuttgart, Germany;
and Group for Computational Life Sciences, Division of Physical Chemistry, Ruđer Bošković Institute, Bijenička 54, 10000, Zagreb, Croatia

Bernd Henning Stumpf
PULS Group, Institut für Theoretische Physik, IZNF, Friedrich-Alexander-Universität Erlangen-Nürnberg, Cauerstraße 3, 91058 Erlangen, Germany

Ana-Sunčana Smith
PULS Group, Institut für Theoretische Physik, IZNF, Friedrich-Alexander-Universität Erlangen-Nürnberg, Cauerstraße 3, 91058 Erlangen, Germany
and Group for Computational Life Sciences, Division of Physical Chemistry, Ruđer Bošković Institute, Bijenička 54, 10000, Zagreb, Croatia

Anna Maciołek
Max-Planck-Institut für Intelligente Systeme Stuttgart, Heisenbergstr. 3, 70569 Stuttgart, Germany
and Institute of Physical Chemistry, Polish Academy of Sciences, Kasprzaka 44/52, 01-224 Warsaw, Poland

(Received 10 June 2022; revised 11 November 2022; accepted 17 April 2023; published 18 May 2023)

We study a model of a lipid bilayer membrane described by two order parameters: the chemical composition described using the Gaussian model and the spatial configuration described with the elastic deformation model of a membrane with a finite thickness or, equivalently, for an adherent membrane. We assume and explain on physical grounds the linear coupling between the two order parameters. Using the exact solution, we calculate the correlation functions and order parameter profiles. We also study the domains that form around inclusions on the membrane. We propose and compare six distinct ways to quantify the size of such domains. Despite its simplicity, the model has many interesting features like the Fisher-Widom line and two distinct critical regions.

DOI: 10.1103/PhysRevE.107.054120

I. INTRODUCTION

Continuous research effort has been put into understanding the relationship between physical properties, functionality, and the mutual influence of lipids and proteins in cell membranes. One of the central issues concerns membrane domains. It is well established that model lipid bilayer membranes containing cholesterol can support two coexisting liquid phases, called liquid-ordered (Lo) and liquid-disordered (Ld) [1–3]. Below the critical point of miscibility domains of different phases form, giving rise to a lateral heterogeneity of a lipid membrane. Formation of domains and functional lateral heterogeneity is observed also in living cell membranes [4–6]. The structure, spatial organization, and role of lipid and protein domains in cell signaling has been a long studied problem. Nevertheless, many questions are still open in this field [7–12]. Observed domains are nanoscopic and dynamical and also occur above the critical point [13–15]; therefore the physical basis of heterogeneity in cell membranes is supposed to be more complex than a miscibility transition alone.

Diverse equilibrium mechanisms that can lead to membrane segregation on length scales smaller than the characteristic size of the bulk phase separation domains have been identified theoretically and experimentally [16,17]. Several of them involve nanometer-sized membrane inclusions, such as proteins. In general, both direct and indirect interactions between inclusion and membrane lipids can generate domains. Direct specific interactions cause chemically favored lipids to be attracted to the protein, creating a wetting domain [18–20] or, above the critical temperature of demixing, an adsorption domain with a concentration of preferred lipids greater than that of the bulk membrane. The extent of the adsorption domain is of the order of the composition correlation length ξ, and thus, near the critical point of demixing, where ξ grows significantly, it can be as large as several microns [21,22].

Here we focus on the indirect interactions resulting from protein-induced membrane disturbances. Among such perturbations are changes due to hydrophobic mismatch between membrane lipids and inclusion, i.e., when the hydrophobic part of the inclusion has a thickness slightly different from the hydrophobic part of the membrane [23,24]. The energetic cost

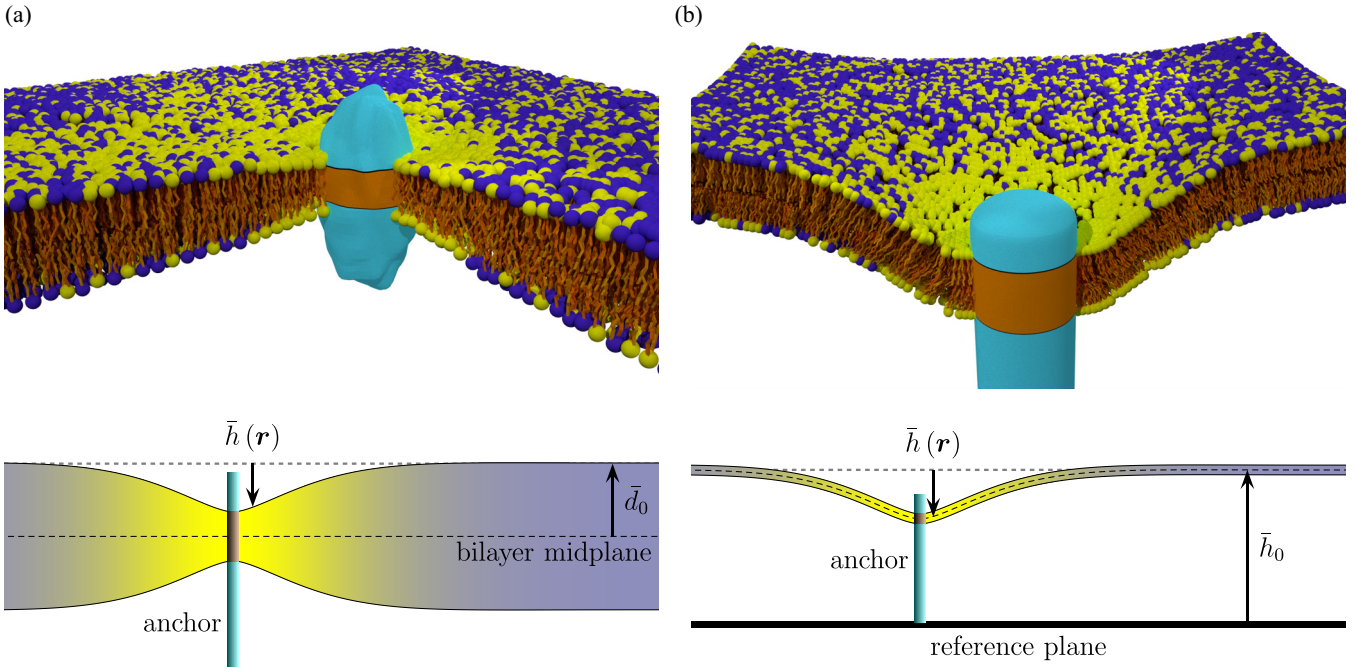

FIG. 1. Schematic plot of the two possible applications of the model. Different types of lipids are denoted with blue and yellow. (a) The membrane is flat, but its thickness is not constant and described by the order parameter $\bar{h}(\boldsymbol{r})$. Due to hydrophobic mismatch of the anchor (difference between the equilibrium thickness of the membrane and size of the hydrophobic region on the anchor) the thickness of the membrane is alerted around the anchor, which modifies local composition of the lipids. (b) The membrane has a constant thickness, but it is not flat, and its height over the reference plane is described by the order parameter $\bar{h}(\boldsymbol{r})$. In this case the anchor (illustrated in the middle of the picture) is locally fixing the height of the membrane, and, as a result, the membrane is bent. The external potential that acts differently on different types of lipids changes the composition of the membrane around the anchor.

of hydrophobic mismatch deformation can be reduced by attracting lipids with a suitable characteristic. One possibility is that lipids that match the curvature of the membrane caused by the protein will be effectively attracted [25–28]. Thus inclusions with a hydrophobic core larger or smaller than that of the membrane would tend to attract lipids of positive or negative spontaneous curvature, thereby building a concave or convex shape to fill in the height mismatch. For example, cholesterol and saturated lipids exhibit a negative spontaneous curvature, whereas unsaturated lipids, with a smaller acyl chain area to polar head group area ratio, exhibit positive spontaneous curvature. In this mechanism, the inclusion-induced deformation is strongly dependent upon the spontaneous curvature, which in turn is coupled to the composition of the membrane.

In this paper we discuss a different possibility for creating chemical inhomogeneity. In order to accommodate hydrophobic mismatch, lipids of matching length of the acyl chain are effectively attracted to the protein inclusion [20]. In model membranes, such as those considered experimentally in Refs. [1–3], the hydrophobic thickness of the membrane is nonuniform. The Lo phase, rich in saturated lipids, shows higher extension in the lipid acyl chains than the Ld phase, rich in unsaturated lipids [29]. Depending on the sign of the hydrophobic mismatch, the lipid composition around the protein will preferentially be in one of the two phases (Lo or Ld). In this mechanism, which we call the thickness mechanism, the composition of the membrane is coupled to its thickness [30,31] and not necessarily to the overall spontaneous curvature of the membrane. This process is schematically illustrated in Fig. 1(a).

Another possible mechanism for creating lipid domains around proteins is relevant in membrane adhesion. In this case we consider the coupling of the lipid composition to a particular separation between the membrane and opposing surface (of another cell or of the extracellular matrix). Two cell or celllike membranes in the absence of protein-mediated adhesion maintain a finite distance of the order of 100 nm [32,33]; hence, the membrane behaves as resting in a potential minimum. This initial separation is regulated through the composition of the membrane and the cell glycocalyx, and changes in these parameters result in different separations. Local change of the separation occurs when bonds form between receptors in the membrane and their binding partners on the opposing cell or in the extracellular environment (ligands or proteins). In order for this bond to take place, the glycocalyx must be expelled [34], which, in turn, leads to a change of the composition of the membrane itself. A schematic plot of this mechanism in presented in Fig. 1(b). Such a process has been observed in integrin or cadherin adhesion [35,36], but the same scenario is responsible for protein organization during the formation of the T-cell synapse [37] or natural killer cell activation [38].

From the theoretical point of view, the curvature effects already were conceptually formalized two decades ago [27]. Further detailed analysis was both performed analytically and in simulations by several groups [39–45]. The thickness mechanism (coupling between the thickness of the membrane

and its composition) was suggested in a numerical study [30], while the analytic approach was then put forward only last year by us [31]. In Ref. [31] we proposed a model which couples the elasticity theory of lipid bilayer thickness deformations [24,30,46,47] with the Landau-Ginzburg theory of a near-critical binary mixture and with the inclusions. Our model can be solved exactly, which has the obvious advantage of allowing for a full understanding of the consequences of considered couplings (beyond curvature) on the local demixing of the binary lipid membrane. The price for this is the simplification of the actual system, including the disregard of the size, shape, and conformation of protein inclusions and other specific properties of lipid bilayers, such as lipid tilt [48] or intrinsic curvature, inhomogeneous deformations of lipid volume, or asymmetric bilayer thickness deformations. We are also restricted to the supercritical range of temperatures. Nevertheless, our minimal model was able to reproduce experimental observations of the formation of lipid domains around lipids linked to a reconstituted actin cortex filament in a model membrane [31,39]. In these experiments the lipid bilayer was supported, which strongly suppresses spontaneous curvature effects.

Interestingly, we note that, following the work of Bibtol *et al.* [24], it is possible to draw a direct analogy between the thickness and the shape deformation of the membrane in the lowest order of theory. That means it is possible, on a different length scale, to address theoretically both problems within the same framework. The role of this paper is to provide this analogy and to describe our model in more detail, which we could not do in the letter format. Furthermore, we want to understand the adsorption of lipids onto the protein inclusion given that no direct attractive interaction is imposed.

We first explore the general features of the model for both the shape and thickness deformation fields by computing and analyzing correlation functions. In the absence of the protein inclusions, we calculate two-point correlation functions and discuss different forms of their asymptotic decay in connection with the poles appearing in their integral representation. Due to the presence of two order parameters and higher order derivatives in the Hamiltonian, the behavior of these functions is rich and interesting. For example, the correlation length that governs the asymptotic decay of the correlation functions shows a curious nonmonotonic and nonanalytic behavior as function of the temperature deviation τ from the critical temperature. This is far from a typical behavior of a binary mixture upon approaching the critical point. From our analytical results we derive the asymptotic behavior of the correlation functions and the correlation length in the several limiting cases of the three relevant parameters of our model.

Furthermore, we investigate adsorption phenomena around membrane-embedded protein in the context of a domain formation upon approaching the critical temperature. Given that there is no direct attraction between proteins and lipids that would be responsible for the classical critical adsorption, it is interesting to understand what kind of universal scaling law is obeyed for the adsorption phenomena that take place entirely due to the coupling of the two order parameters. For this purpose we calculate the order parameter profiles around protein inclusion. Based on the integral and local properties of these profiles, we propose several definitions of the size of the domain. We determine their asymptotic behavior in several limits, including approaching the critical temperature ($\tau \to 0$).

Our minimal model does not include membrane tension. We show under which conditions taking into account the surface tension does not qualitatively change the results of our model.

The paper is organized as follows: In Sec. II we define the model, explain the physical mechanisms behind our assumptions, and briefly explain the method of calculation. Section III is devoted to the correlation functions. We define them and use their properties to distinguish three zones in the space of the parameters. In Sec. IV we discuss the order parameter profiles and study the formation of domains. We introduce and compare six different ways to identify the size of induced domains. Our research is summarized and discussed in Sec. V. Finally, we have included several Appendixes: in Appendix A we discuss how the properties of our model change for nonzero surface tension; Appendix B presents the method used to calculate the order parameter profiles and correlation functions; in Appendix C we discuss the behavior of the roots of a certain polynomial, which determine the properties of correlation functions; in Appendix D we present the details of the calculation of the integrals present in the formulas for the correlation functions in different zones; and, finally, in Appendix E we study the correlation functions in various limiting cases.

II. MODEL

We start from introducing the model discussed in this paper. In order to describe the system we use two order parameters.

A. Configuration order parameter

The spatial configuration of the membrane is described by the order parameter $\bar{h}(\boldsymbol{r})$, the height of the membrane above the reference plane in a point given by the two-dimensional vector $\boldsymbol{r}$. For simplicity we assume that the membrane is infinite, such that $\boldsymbol{r}$ can be any vector from the plane. The energy associated with the configuration of a membrane can be approximated by [49–52]

$$\beta\mathcal{H}_{\mathrm{MD}} = \int d\boldsymbol{r}\{2\kappa[\mathrm{H}(\boldsymbol{r})]^2 + \eta\,\mathrm{S}(\boldsymbol{r}) + V_{\mathrm{ext}}[\bar{h}(\boldsymbol{r})]\}, \quad (1)$$

which we call the membrane deformation model. In this Hamiltonian the bending stiffness κ is a dimensionless parameter describing the energy cost of bending the membrane, $\mathrm{H}(\boldsymbol{r})$ is a mean curvature of the membrane, η denotes the surface tension, $\mathrm{S}(\boldsymbol{r})$ is a local change in surface area due to membrane deformation, and an external potential V_{ext} keeps the membrane above the reference plane. In (1) we have introduced $\beta = (k_{\mathrm{B}}T)^{-1}$ (where T is a temperature and k_B is the Boltzmann constant) in order to keep the formula dimensionless, and we have assumed that the membrane has no spontaneous curvature.

When the membrane is almost flat, i.e., $|\nabla\bar{h}(\boldsymbol{r})| \ll 1$, the mean curvature $\mathrm{H}(\boldsymbol{r}) \approx \nabla^2\bar{h}(\boldsymbol{r})/2$, and the local change in surface area $\mathrm{S}(\boldsymbol{r}) \approx [\nabla\bar{h}(\boldsymbol{r})]^2/2$. The external potential originates

from many different interactions like steric repulsion or van der Waals attraction and, in cellular systems, from the properties of the glycocalyx. We assume that it has a minimum for $\bar{h} = \bar{h}_0$, and (since we are interested only in small excitations around the minimum) it can be approximated by a harmonic potential. If one, for simplicity, additionally assumes that its minimum is at $\bar{h} = 0$, $V_{\text{ext}} \approx \gamma \bar{h}^2/2$, where the parameter γ quantifies the strength of binding of the membrane.

The energy of a flat membrane with a variable thickness can also be approximated by Eq. (1) for $|\nabla \bar{h}(\boldsymbol{r})| \ll 1$. We assume that a bilayer membrane is symmetric, so that the thickness deformations of the two monolayers are identical. In this picture, the order parameter $\bar{h}(\boldsymbol{r})$ is defined as the difference between the local thickness and the thickness $\bar{d}_0$ of an unperturbed membrane (i.e., the distance between two lipid layers). Of course, in this interpretation the meaning of κ and V_{ext} is different: the parameter κ, as shown in [24], is four times smaller than the true bending stiffness of the membrane, and the potential now describes the interaction between the two layers: it regulates the energy cost of the compression or expansion of the lipid bilayer. Both possible interpretations of the order parameter $\bar{h}(\boldsymbol{r})$ have been schematically illustrated in Fig. 1.

A comprehensive description of a membrane definitely requires consideration of both the spatial configuration of the membrane and its thickness by taking into account two distinct configuration order parameters [24] (in the leading order they decouple from each other in the formula for a total elastic energy of the membrane). In this paper, in order to keep the model as simple as possible, we use only a single field $\bar{h}(\boldsymbol{r})$. Nevertheless, we keep two possible interpretations as they are both experimentally relevant.

To make our model simpler we also assume that the effects of surface tension can be neglected (we take $\eta = 0$). While, when $\bar{h}(\boldsymbol{r})$ denotes the spatial configuration of the membrane, this assumption is reasonable as in most cases the effect of surface tension effectively modifies other parameters describing the membrane [53], the situation is more subtle when $\bar{h}(\boldsymbol{r})$ denotes the thickness of the membrane. In this case the surface area term in $\beta\mathcal{H}_{\text{MD}}$ [Eq. (1)] gives rise to two leading contributions $\bar{h}(\boldsymbol{r})/\bar{d}_0$ and $[\nabla \bar{h}(\boldsymbol{r})]^2$, which were employed in the literature to describe the effects of stretching deformations tangential to the leaflet surfaces (typically by fixing the volume of the membrane per molecule) and changes in the projection of the bilayer area onto the reference plane, respectively [24,30,48,54,55]. As shown in Ref. [24], there appears another term proportional to $[\nabla \bar{h}(\boldsymbol{r})]^2$ if one takes into account the energy cost due to an increase of the area per molecule in deformed membrane. It was argued that the amplitude of this term results from the interfacial tension of the hydrocarbon-water interface, which is of the order of 40–50 mN/m. This is much larger than the estimated maximum membrane tension (just before its rupture), which is of the order of a few mN/m.

In Appendix A we investigate how our results would change if we included the surface tension in the model. We show that as long as the relevant parameter $\vartheta = \eta/\sqrt{\kappa\gamma} < 2$, the effect of surface tension is generating only a minor quantitative change. Moreover, even if $\vartheta \geqslant 2$, where the qualitative change occurs (the oscillatory solutions for the correlation functions and order parameter profiles disappear), our results for exponentially decaying functions are still valid.

Our estimates based on the values of parameters reported in literature [24,54] are that for real bilipid membranes, when $\bar{h}$ denotes the thickness of the membrane, the coefficient ϑ is of the order of 1, so our model should be valid at least for some membranes [56]. When $\bar{h}$ denotes the spatial position of the membrane, ϑ depends strongly on the experimental setup (via η and γ), but we expect it to be even smaller.

B. Composition order parameter

In order to describe the composition of the membrane we introduce a scalar order parameter $\bar{\phi}(\boldsymbol{r})$. We define it as a difference between the local concentration of saturated lipids and their concentration at the critical demixing point. In this way, above the critical temperature T_{c} the equilibrium value of the order parameter is zero, and below T_{c} it has two possible equilibrium values: the positive describing Lo phase and negative describing Ld phase.

In this paper we use only one composition order parameter to describe the membrane in order to keep the model simple; thorough description of the chemical composition would require the introduction of several order parameters (separately for each component and each layer), which typically complicates the phase diagram.

Around the critical point, the energy associated with the chemical composition can be approximated by the Landau-Ginzburg Hamiltonian

$$\beta\mathcal{H}_{\text{LG}} = \int d\boldsymbol{r}\left\{\frac{\sigma}{2}[\nabla\bar{\phi}(\boldsymbol{r})]^2 + t\bar{\phi}^2(\boldsymbol{r}) + u\bar{\phi}^4(\boldsymbol{r}) - c\bar{\phi}(\boldsymbol{r})\right\}, \tag{2}$$

where $\sigma > 0$ measures the energy cost of a chemical gradient on the membrane, $t \propto T - T_{\text{c}}$ is the temperature, $u > 0$, and c is the ordering field proportional to the deviation of the chemical potential of the considered component from its critical value.

In our model for the sake of simplicity, we assume that $c = 0$ and $u = 0$ in Eq. (2). The former means that the composition of the membrane is at its critical-point value, which seems to be in line with some of the experiments [39]. The latter assumption makes the Hamiltonian unbounded from below for $t < 0$ and, therefore, restricts our analysis to the cases where the membrane is in a mixed state ($t > 0$). For $u > 0$ an analytical solution of our model is not known.

The two remaining terms in Hamiltonian (2) ($u = 0$, $c = 0$ and $t > 0$) define the so-called Gaussian model [51].

C. Coupling between order parameters

In order to study the relation between the chemical composition and shape of the membrane, it is necessary to introduce coupling between the order parameters.

The simplest, mathematical coupling arises from the observation that the integral in Landau-Ginzburg Hamiltonian (2) should be calculated on the curved manifold [given by $\bar{h}(\boldsymbol{r})$] rather than on the flat reference plain. Close investigation shows that this effect gives corrections that are proportional to

the powers of $\nabla\bar{h}$, and thus they are not relevant in the limit of an almost flat surface $|\nabla\bar{h}(\boldsymbol{r})| \ll 1$ assumed in our model.

The physical mechanism of coupling between the order parameter $\bar{\phi}$ and the mean curvature H of the membrane was proposed and analyzed in Refs. [25,57]. In the leading order, it gives a coupling in Hamiltonian that is proportional to $\bar{\phi}\nabla^2\bar{h}$, which can lead to a curvature-driven phase separation in the membrane.

In this paper we propose a different physical mechanism that leads to a direct coupling between the order parameters—a term proportional to $\bar{h}\bar{\phi}$ in the Hamiltonian.

When $\bar{h}$ describes the spatial configuration of the membrane, an external potential V_{ext} [see Eq. (1)] represents a nonspecific adhesion, which keeps the membrane shape in a minimum of an effective potential. Various theoretical and experimental studies [58–62] indicate that the strength and the position of this nonspecific minimum results from balancing the membrane-substrate van der Waals and the Coulomb potential with the membrane deformation repulsion. Other types of interactions could also contribute. The quadratic form of V_{ext} is thought of as an expansion of the effective potential around its minimum. It is natural to assume that that this effective potential depends on the composition $\bar{\phi}$ (e.g., via van der Waals interactions [62]). The simplest possible way to include this effect is to consider the composition-dependent equilibrium height of the membrane, which for small $|\bar{\phi}|$ gives

$$V_{\text{ext}} = \frac{\gamma}{2}[\bar{h}(\boldsymbol{r}) - \alpha\bar{\phi}(\boldsymbol{r})]^2, \tag{3}$$

where we have introduced the proportionality coefficient α.

On the other hand, when $\bar{h}$ denotes the excess thickness of the membrane (over the reference value $\bar{d}_0$) we assume that different lipids have a different effective length of acyl chains. This makes the equilibrium thickness of the bilayer dependent on its chemical composition and justifies Eq. (3).

The effect of the coupling between order parameters has been schematically shown in Fig. 1 for both possible interpretations of $\bar{h}$.

We note that from the point of view of the composition order parameter $\bar{\phi}$, the coupling term given by Eq. (3) has two effects: the term quadratic in $\bar{\phi}$ effectively shifts t by $\alpha^2\gamma/2$ (and therefore pushes the system away from the critical point), and the term linear in $\bar{\phi}$ represents a position-dependent [via $\bar{h}(\boldsymbol{r})$] chemical potential.

D. Inclusions

Finally, we introduce inclusions that model the anchors (like proteins or lipids) immersed in the membrane. We assume that they are coupled to the configuration order parameter: If $\bar{h}$ is the height of the membrane above the reference plane, we assume that the inclusions are attached to some external structures (cytoskeleton) and deform locally the shape of the membrane. If $\bar{h}$ denotes the thickness of the membrane, we assume that the inclusions have a hydrophobic mismatch, i.e., the hydrophobic region on the inclusion has a different height than the height of the unperturbed membrane. As a result the membrane gets thicker or thinner close to the inclusion.

For simplicity we neglect the size of inclusions and assume that they are all isotropic and pointlike [63,64]. As a first approximation, we also neglect the possible different affinities to different components of the membrane, i.e., coupling of the inclusion directly to order parameter $\bar{\phi}$. This effect is worth studying separately, but we expect it to be subdominant in comparison with coupling to $\bar{h}$. A more realistic model would require introducing some nonzero area covered by the inclusion [this area should be excluded from the integrals in Eqs. (1) and (2), as the order parameters are undefined there] and taking into account a possibility of angle-dependent coupling. Moreover, the details of an interaction between an inclusion and the membrane have been studied only for a limited number of cases, and they often are under debate. Pointlike inclusions are described with only a few parameters (like the values of order parameters and their derivatives) that can be fitted to reproduce a correct long distance behavior of the membrane observed around the real inclusion. The price to pay for this simplification is the possibility that some quantities will be divergent. In our model, allowing for pointlike inclusions coupled to $\bar{\phi}$ leads to some divergent integrals and requires introducing a regularization scheme, which we discuss in more detail in Sec. IV.

We denote by N the number of inclusions and label their positions by $\boldsymbol{r}_1, \boldsymbol{r}_2, \ldots, \boldsymbol{r}_N$. We approximate the interaction with the harmonic potential:

$$\beta\mathcal{H}_{\text{I}} = \frac{\lambda}{2}\sum_{i=1}^{N}[\bar{h}(\boldsymbol{r}_i) - \bar{h}_i]^2, \tag{4}$$

where $\bar{h}_i$ denotes the value of $\bar{h}$ preferred by ith inclusion, and the positive coefficient λ defines the strength of the potential. In our calculations, for the sake of simplicity, we take the limit $\lambda \to \infty$, which enforces the relations $\bar{h}(\boldsymbol{r}_i) = \bar{h}_i$ for $i = 1, 2, \ldots, N$.

E. Hamiltonian of the model

We can now write the full Hamiltonian of our model in the reduced, dimensionless variables.

We use the length scale

$$\zeta = (\kappa/\gamma)^{1/4} \tag{5}$$

as a unit of length, and define $h = \bar{h}/\zeta$ and $\boldsymbol{\rho} = \boldsymbol{r}/\zeta$. The length scale ζ is proportional [65] to the correlation length in a model of a tensionless membrane with a single order parameter $\bar{h}(\boldsymbol{r})$ [66]. The unit of the composition is given by $\sigma^{-1/2}$, and the unit of energy is $k_{\text{B}}T$. All the formulas for dimensionless variables are summarized in Table I.

There are three dimensionless parameters that describe our model: the bending stiffness κ which is already dimensionless in the original formula, the reduced dimensionless temperature $\tau = t\zeta^2/\sigma$ proportional to the reduced temperature t, and the parameter $\mu = \alpha\sigma^{-1/2}/\zeta$ that is proportional to the coupling α between the order parameters. It is also convenient to introduce a fourth parameter $\omega = \kappa\mu^2 = \kappa\alpha^2/(\sigma\zeta^2)$ as this combination of parameters often appears in our formulas. As we discuss in Sec. II F, this parameter regulates the length scale starting from which the thermal fluctuations of the order parameters must be correlated. The anchors immersed in

TABLE I. Definition of dimensionless parameters used in the model. The unit of length is denoted by L, the unit of chemical composition (the unit of $\bar{\phi}$) is denoted by C, and the unit of energy is denoted by E. In the last column, the names of the reduced variables that we use are given.

Variable	Original unit	Rescaled variable	Name
$\bar{h}$	L	$h = \bar{h}/\zeta$	Reduced height or thickness of the membrane
$\bar{\phi}$	C	$\phi = \bar{\phi}\,\sigma^{1/2}$	Reduced composition of the membrane
$\bar{A}$	L^2	$A = \bar{A}/\zeta^2$	Reduced area of the system
$\mathbf{r}$	L	$\boldsymbol{\rho} = \mathbf{r}/\zeta$	Reduced distance or position
κ	1	κ	Bending stiffness
γ	L^{-4}	–	Strength of the potential acting on the membrane
η	L^{-2}	$\vartheta = \eta/\sqrt{\kappa\gamma}$	Reduced surface tension of the membrane
σ	C^{-2}	–	Parameter describing energy cost of the gradient of concentration
t	$L^{-2}C^{-2}$	$\tau = t\,\zeta^2/\sigma$	Reduced temperature
α	LC^{-1}	$\mu = \alpha\,\sigma^{-1/2}/\zeta$	Reduced coupling
–	1	$\omega = \kappa\mu^2 = \kappa\alpha^2/(\sigma\zeta^2)$	Combination of parameters appearing in the polynomial W
λ	L^{-2}	$\nu = \lambda\zeta^2$	Reduced harmonic potential coefficient
$\bar{h}_i$	L	$h_i = \bar{h}_i/\zeta$	Reduced height of the membrane for proteins

the membrane introduce additional parameters: the positions of anchors $\boldsymbol{\rho}_i$, the imposed reduced heights of the membrane $h_i = \bar{h}_i/\zeta$ for $i = 1, \ldots, N$, and the harmonic potential constant ν (which we set infinite in our calculation). The Hamiltonian in the new variables takes the form

$$\mathcal{H}[h(\boldsymbol{\rho}), \phi(\boldsymbol{\rho})] = \mathcal{H}_{\mathrm{MD}} + \mathcal{H}_{\mathrm{G}} + \mathcal{H}_{\mathrm{C}} + \mathcal{H}_{\mathrm{I}}, \tag{6a}$$

$$\beta\mathcal{H}_{\mathrm{MD}} = \int d\boldsymbol{\rho}\,\frac{\kappa}{2}[\nabla^2 h(\boldsymbol{\rho})]^2, \tag{6b}$$

$$\beta\mathcal{H}_{\mathrm{G}} = \int d\boldsymbol{\rho}\left\{\frac{1}{2}[\nabla\phi(\boldsymbol{\rho})]^2 + \tau\phi^2(\boldsymbol{\rho})\right\}, \tag{6c}$$

$$\beta\mathcal{H}_{\mathrm{C}} = \int d\boldsymbol{\rho}\,\frac{\kappa}{2}[h(\boldsymbol{\rho}) - \mu\phi(\boldsymbol{\rho})]^2, \tag{6d}$$

$$\beta\mathcal{H}_{\mathrm{I}} = \frac{\nu}{2}\sum_{i=1}^{N}[h(\boldsymbol{\rho}_i) - h_i]^2, \tag{6e}$$

where the symbol "∇" denotes the gradient operator in dimensionless variable $\boldsymbol{\rho}$.

In the above formulas: $\mathcal{H}_{\mathrm{MD}}$ describes the energy related to the curvature of the membrane, which is part of the membrane deformation Hamiltonian (1), and, in fact, it is the Hamiltonian expanded in small gradients of h with vanishing surface tension η; $\mathcal{H}_{\mathrm{G}}$ is the Hamiltonian of the Gaussian model, i.e., Eq. (2), with $u = 0$ and $c = 0$; $\mathcal{H}_{\mathrm{C}}$, describing the coupling, originates from the second part of the membrane deformation Hamiltonian with the potential given by Eq. (3); and $\mathcal{H}_{\mathrm{I}}$ is the rescaled version of Eq. (4).

We note that in our model there is no external potential that keeps h close to 0. Instead, this condition is attained via the coupling term (6d), since the order parameter ϕ is kept close to zero (for $\tau > 0$) by the term (6c). As we have checked, adding external potential proportional to $h^2(\boldsymbol{r})$ is not changing basic properties of the system, and, therefore, we do not include it in our model for the sake of simplicity.

We also note that in our model we allow the order parameters to take any real value. Physically, the height of the membrane above the reference plane is always restricted by some objects present in the system. Also, the excess thickness is bounded from below as the two layers of the membrane cannot intersect. Similarly, the concentration of one of the lipids ϕ is bounded by the finite values that describe a membrane without or full of this lipid. Here we ignore this limits in order to solve the model analytically. As an *a posteriori* justification of this assumption, we note that the boundary values of the order parameters are typically located far in the tail of the calculated Gaussian distributions, and, therefore, the nonphysical values are highly improbable.

F. Length scales

Before going to the calculation of the correlation functions, it is useful to discuss the length scales present in our model. We have identified three physically relevant length scales.

The natural length scale for the order parameter $\bar{h}$ is $\ell_h = \sqrt{2}\zeta = (4\kappa/\gamma)^{1/4}$, i.e., the correlation length of the model of the membrane without the composition order parameter $\bar{\phi}$. Analogously, the natural length scale for the order parameter $\bar{\phi}$ is $\ell_\phi = (2\tau)^{-1/2}\zeta = \sqrt{\sigma/(2t)}$, which is the correlation length in the Gaussian model. The third length scale $\ell_{\mathrm{coupling}} = \omega^{-1/2}\zeta = \alpha^{-1}\sqrt{\sigma/\gamma}$ is associated with the coupling between the order parameters. As we have checked, the fluctuation of $\bar{\phi}$ of the size $\sim\ell_{\mathrm{coupling}}$ has the coupling interaction energy [given by $\mathcal{H}_{\mathrm{C}}$; see (6d)] of the order of $1k_{\mathrm{B}}T$. This means that on the scales much smaller than ℓ_{coupling} one can ignore the coupling, while on much larger scales the fluctuations of $\bar{\phi}$ and $\bar{h}$ must be correlated.

The situation changes slightly when one considers nonvanishing surface tension of the membrane, i.e., nonzero η in Eq. (1). In this case the correlation length of the model without the composition order parameter becomes a function of κ, η, and γ [53], and it is not equal to ℓ_h anymore. In such a case one can introduce one more length scale $\ell_{\mathrm{surface\ tension}} = \sqrt{\eta/(2\gamma)}$, which is equal to the correlation length in the special case of $\kappa = 0$. All calculations presented in this paper assume $\eta = 0$, and, therefore, they are valid in the case $\ell_{\mathrm{surface\ tension}} \ll \ell_h, \ell_\phi, \ell_{\mathrm{coupling}}$.

Our exact analysis of the model is valid for any values of the length scales ℓ_h, ℓ_ϕ, and ℓ_{coupling}. In Sec. III G and

Appendix E we discuss the correlation functions in several limiting cases in which one of these length scales becomes much larger or much smaller than others.

G. Method of calculation

The partition function of the system is defined using the path integral over all configurations of the two fields

$$\mathcal{Q}\big(\kappa, \tau, \mu, A; \{h_i, \boldsymbol{\rho}_i\}_{i=1}^N\big) = \int \mathcal{D}h(\boldsymbol{\rho})\mathcal{D}\phi(\boldsymbol{\rho}) \exp\big[-\beta\mathcal{H}\big(\kappa, \tau, \mu, A; \{h_i, \boldsymbol{\rho}_i\}_{i=1}^N\big)\big]. \tag{7}$$

Since all terms in the Hamiltonian (6) are quadratic in the order parameters and their derivatives, it is possible to calculate the partition function analytically—we replace the fields $h(\boldsymbol{\rho})$ and $\phi(\boldsymbol{\rho})$ with their Fourier transforms and calculate the integrals separately for every wave vector. For the details of this procedure as well as for the calculation of the correlation functions and order parameters profiles see Appendix B.

III. CORRELATION FUNCTIONS

A. Definition

We start the investigation from studying the two-point correlation functions in the system without proteins. For such a system $N = 0$, the Hamiltonian is

$$\mathcal{H} = \mathcal{H}_{\mathrm{MD}} + \mathcal{H}_{\mathrm{G}} + \mathcal{H}_{\mathrm{C}}, \tag{8}$$

where the terms on the right-hand side are given by Eq. (6). Because of the symmetry of changing the sign of both order parameters, $\langle h(\boldsymbol{\rho})\rangle = \langle\phi(\boldsymbol{\rho})\rangle = 0$ for any position $\boldsymbol{\rho}$. Therefore, we define all the possible two-point correlation functions via

$$\mathfrak{C}_{hh}(\rho;\kappa,\tau,\mu) = \langle h(\boldsymbol{\rho}_0)h(\boldsymbol{\rho}_0+\boldsymbol{\rho})\rangle, \tag{9a}$$

$$\mathfrak{C}_{h\phi}(\rho;\kappa,\tau,\mu) = \langle h(\boldsymbol{\rho}_0)\phi(\boldsymbol{\rho}_0+\boldsymbol{\rho})\rangle, \tag{9b}$$

$$\mathfrak{C}_{\phi\phi}(\rho;\kappa,\tau,\mu) = \langle \phi(\boldsymbol{\rho}_0)\phi(\boldsymbol{\rho}_0+\boldsymbol{\rho})\rangle. \tag{9c}$$

Since the Hamiltonian (8) is invariant under rotations and translations, these functions depend only on the length ρ of the vector $\boldsymbol{\rho}$, and they are independent of the reference point $\boldsymbol{\rho}_0$.

B. Integral formulas for the correlation functions

Using the path integral method, we obtain the formulas for the correlation functions (see Appendix B 1)

$$\mathfrak{C}_{hh}(\rho;\kappa,\tau,\mu) = \frac{1}{2\pi\kappa}\int_0^\infty \frac{x(x^2+\omega+2\tau)\mathcal{J}_0(\rho x)}{(x^4+1)(x^2+2\tau+\omega)-\omega}\,dx, \tag{10a}$$

$$\mathfrak{C}_{h\phi}(\rho;\kappa,\tau,\mu) = \frac{\mu}{2\pi}\int_0^\infty \frac{x\,\mathcal{J}_0(\rho x)}{(x^4+1)(x^2+2\tau+\omega)-\omega}\,dx, \tag{10b}$$

$$\mathfrak{C}_{\phi\phi}(\rho;\kappa,\tau,\mu) = \frac{1}{2\pi}\int_0^\infty \frac{x(x^4+1)\mathcal{J}_0(\rho x)}{(x^4+1)(x^2+2\tau+\omega)-\omega}\,dx, \tag{10c}$$

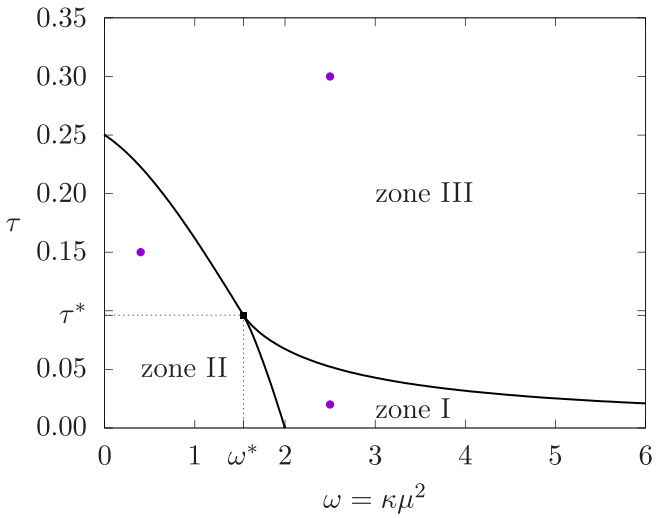

FIG. 2. Plot of the three zones in the space of parameters defined by the properties of roots of the polynomial $W(z;\tau,\kappa\mu^2)$; see Eq. (11). The behavior of the correlation functions for large ρ is different in each zone. The blue dots denote the values of parameters used in Fig. 3, and the black square marks the point where all three zones meet $(\omega^*, \tau^*) = (8/(3\sqrt{3}), 1/(6\sqrt{3}))$.

where $\mathcal{J}_i$ denotes the (unmodified) Bessel function of the first kind of order i, and $\omega = \kappa\mu^2$.

C. Three zones

The above integrals can be transformed to contour integrals on the complex plane and calculated using the residue theorem [67]. The final formula depends on the form of complex roots of the polynomial in complex variable z,

$$W(z;\omega,\tau) = (z^4+1)(z^2+2\tau+\omega)-\omega, \tag{11}$$

which is in the denominator of all the integrands in (10). Since $W(z;\omega,\tau)$ has real coefficients and only even powers of z, if z_0 is its root, then z_0^*, $-z_0$ and $-z_0^*$ are the roots of W (the symbol z^* denotes the complex conjugate of a number z). This polynomial has no real roots.

The plane of the parameters (ω,τ) is split into three different zones by the properties of the roots of the polynomial $W(z;\omega,\tau)$. In zone I the polynomial has only imaginary roots $\pm it_1$, $\pm it_2$, and $\pm it_3$, where we assume $0 < t_1 < t_2 < t_3$. In zone II there are two imaginary roots $\pm it_1$ and four complex roots of a form $\pm a \pm it_2$, with $a, t_1, t_2 > 0$, and $t_1 < t_2$. Finally, in zone III the roots are of the same form as in zone II, $\pm it_1$ and $\pm a \pm it_2$ with $a, t_1, t_2 > 0$, but now $t_1 > t_2$. The splitting of the parameter plane is presented in Fig. 2.

The behavior of the roots upon crossing the boundaries of the zones is discussed in Appendix C.

D. Explicit formulas in three zones

Using the parameters describing roots of the polynomial W, we were able to calculate the integrals in Eq. (10) to obtain explicit formulas for the correlation functions.

In *zone I*, where all the roots of the polynomial (11) are imaginary, the correlation functions are

$$\mathfrak{C}_{hh}(\rho;\kappa,\tau,\mu)=\frac{1}{2\pi\kappa}\left[\frac{\mathcal{M}(\rho,t_1)\left(2\tau+\omega-t_1^2\right)}{\left(t_1^2-t_2^2\right)\left(t_1^2-t_3^2\right)}+\frac{\mathcal{M}(\rho,t_2)\left(2\tau+\omega-t_2^2\right)}{\left(t_2^2-t_1^2\right)\left(t_2^2-t_3^2\right)}+\frac{\mathcal{M}(\rho,t_3)\left(2\tau+\omega-t_3^2\right)}{\left(t_3^2-t_1^2\right)\left(t_3^2-t_2^2\right)}\right], \tag{12a}$$

$$\mathfrak{C}_{h\phi}(\rho;\kappa,\tau,\mu)=\frac{\mu}{2\pi}\left[\frac{\mathcal{M}(\rho,t_1)}{\left(t_1^2-t_2^2\right)\left(t_1^2-t_3^2\right)}+\frac{\mathcal{M}(\rho,t_2)}{\left(t_2^2-t_1^2\right)\left(t_2^2-t_3^2\right)}+\frac{\mathcal{M}(\rho,t_3)}{\left(t_3^2-t_1^2\right)\left(t_3^2-t_2^2\right)}\right], \tag{12b}$$

$$\mathfrak{C}_{\phi\phi}(\rho;\kappa,\tau,\mu)=\frac{1}{2\pi}\left[\frac{\mathcal{K}_0(\rho t_1)\left(t_1^4+1\right)}{\left(t_1^2-t_2^2\right)\left(t_1^2-t_3^2\right)}+\frac{\mathcal{K}_0(\rho t_2)\left(t_2^4+1\right)}{\left(t_2^2-t_1^2\right)\left(t_2^2-t_3^2\right)}+\frac{\mathcal{K}_0(\rho t_3)\left(t_3^4+1\right)}{\left(t_3^2-t_1^2\right)\left(t_3^2-t_2^2\right)}\right], \tag{12c}$$

where we have introduced the function

$$\mathcal{M}(\rho,t)=\begin{cases}\mathcal{K}_0(\rho\,t) & \text{for} \quad \rho>0,\\ -\ln t & \text{for} \quad \rho=0,\end{cases} \tag{13}$$

and $\mathcal{K}_i$ is a modified Bessel function of the second kind of order i. Even though $\mathcal{M}$ is not continuous in ρ, the correlation functions $\mathfrak{C}_{hh}$ and $\mathfrak{C}_{h\phi}$ are continuous at $\rho=0$ (the divergent terms in the expansion of Bessel functions cancel each other). The correlation function $\mathfrak{C}_{\phi\phi}$ diverges logarithmically for small ρ,

$$\mathfrak{C}_{\phi\phi}(\rho;\kappa,\tau,\mu)=-\frac{\ln\rho}{2\pi}+O(1), \quad \text{for } \rho\to 0, \tag{14}$$

and the integral (10c) is divergent for $\rho=0$. These properties of the correlation functions for $\rho\to 0$ are true in all zones; they are remnants of the divergences present in the Gaussian model in two dimensions [68].

Each of the correlation functions in Eq. (12) consist of three terms. When ρ is large these terms decay to zero exponentially with length scales, respectively, $1/t_1$, $1/t_2$, and $1/t_3$; and since in this zone $t_1<t_2<t_3$, the first term dominates over two other terms. Therefore, in this zone the correlation length $\xi=1/t_1$.

In *zone II* the correlation functions are

$$\mathfrak{C}_{hh}(\rho;\kappa,\tau,\mu)=\frac{1}{2\pi\kappa}\left[\frac{\mathcal{M}(\rho,t_1)\left(2\tau+\omega-t_1^2\right)}{\left(t_1^2-t_2^2\right)^2+2a^2\left(t_1^2+t_2^2\right)+a^4}-\operatorname{Im}\left(\frac{\mathcal{M}(\rho,t_2+ia)[(a-it_2)^2+2\tau+\omega]}{2at_2\left[t_1^2+(a-it_2)^2\right]}\right)\right], \tag{15a}$$

$$\mathfrak{C}_{h\phi}(\rho;\kappa,\tau,\mu)=\frac{\mu}{2\pi}\left[\frac{\mathcal{M}(\rho,t_1)}{\left(t_1^2-t_2^2\right)^2+2a^2\left(t_1^2+t_2^2\right)+a^4}-\operatorname{Im}\left(\frac{\mathcal{M}(\rho,t_2+ia)}{2at_2\left[t_1^2+(a-it_2)^2\right]}\right)\right], \tag{15b}$$

$$\mathfrak{C}_{\phi\phi}(\rho;\kappa,\tau,\mu)=\frac{1}{2\pi}\left[\frac{\mathcal{K}_0(\rho t_1)\left(t_1^4+1\right)}{\left(t_1^2-t_2^2\right)^2+2a^2\left(t_1^2+t_2^2\right)+a^4}-\operatorname{Im}\left(\frac{\mathcal{K}_0[\rho(t_2+ia)][(a-it_2)^4+1]}{2at_2\left[t_1^2+(a-it_2)^2\right]}\right)\right], \tag{15c}$$

where the function $\mathcal{M}(\rho,t)$ is given by (13). Like in the previous case, the functions $\mathfrak{C}_{hh}$ and $\mathfrak{C}_{h\phi}$ are continuous for $\rho=0$ and $\mathfrak{C}_{\phi\phi}$ diverges for $\rho\to 0$; see Eq. (14).

For large ρ the two terms present in all the formulas for the correlation functions (15) decay to zero like $\exp(-t_1\rho)$ and $\exp(-t_2\rho)$, respectively. Because in this zone $t_1<t_2$, the first term dominates over the second one, and the correlation length $\xi=1/t_1$.

Finally, in *zone III* the correlation functions are given by Eq. (15), the same as in the previously discussed zone II. The reason for this similarity is the same mathematical structure of the roots of the polynomial (11) in these two zones. However, in this zone $t_1>t_2$, and, therefore, for large ρ the second terms in the formulas (15) dominate; the correlation length ξ is $1/t_2$. The difference between dominating terms justifies the distinction we have made between zones II and III.

It is convenient to decompose the correlation functions in all of the zones into a dominating decay and an amplitude

$$\mathfrak{C}_{xx}(\rho;\kappa,\tau,\mu)=\mathcal{A}_{xx}(\rho;\kappa,\tau,\mu)\rho^{-1/2}e^{-\rho/\xi(\omega,\tau)}, \tag{16}$$

where "xx" denotes "hh", "$h\phi$," or "$\phi\phi$", $\mathcal{A}_{xx}$ are the amplitudes, and the correlation length

$$\xi(\tau,\omega)=\begin{cases}1/t_1(\tau,\omega) & \text{in zones I and II},\\ 1/t_2(\tau,\omega) & \text{in zone III},\end{cases} \tag{17}$$

will be discussed in the next subsection.

The three amplitudes $\mathcal{A}_{xx}$ are zero for $\rho=0$ [in the case of $\mathfrak{C}_{\phi\phi}$, the divergence for $\rho\to 0$ is cured by the factor $\rho^{-1/2}$ present in Eq. (16)]. The behavior of the amplitudes for $\rho>0$ is different in different zones. In zone I the amplitudes monotonically increase upon increasing ρ, and their value saturates at certain limiting values attained for $\rho\to\infty$. In zone II the amplitudes also have a well-defined limit for $\rho\to\infty$, but they show some oscillations caused by the second term in each of the formulas (15). These oscillations decay with a length scale $1/t_2$ and typically make the amplitude nonmonotonic

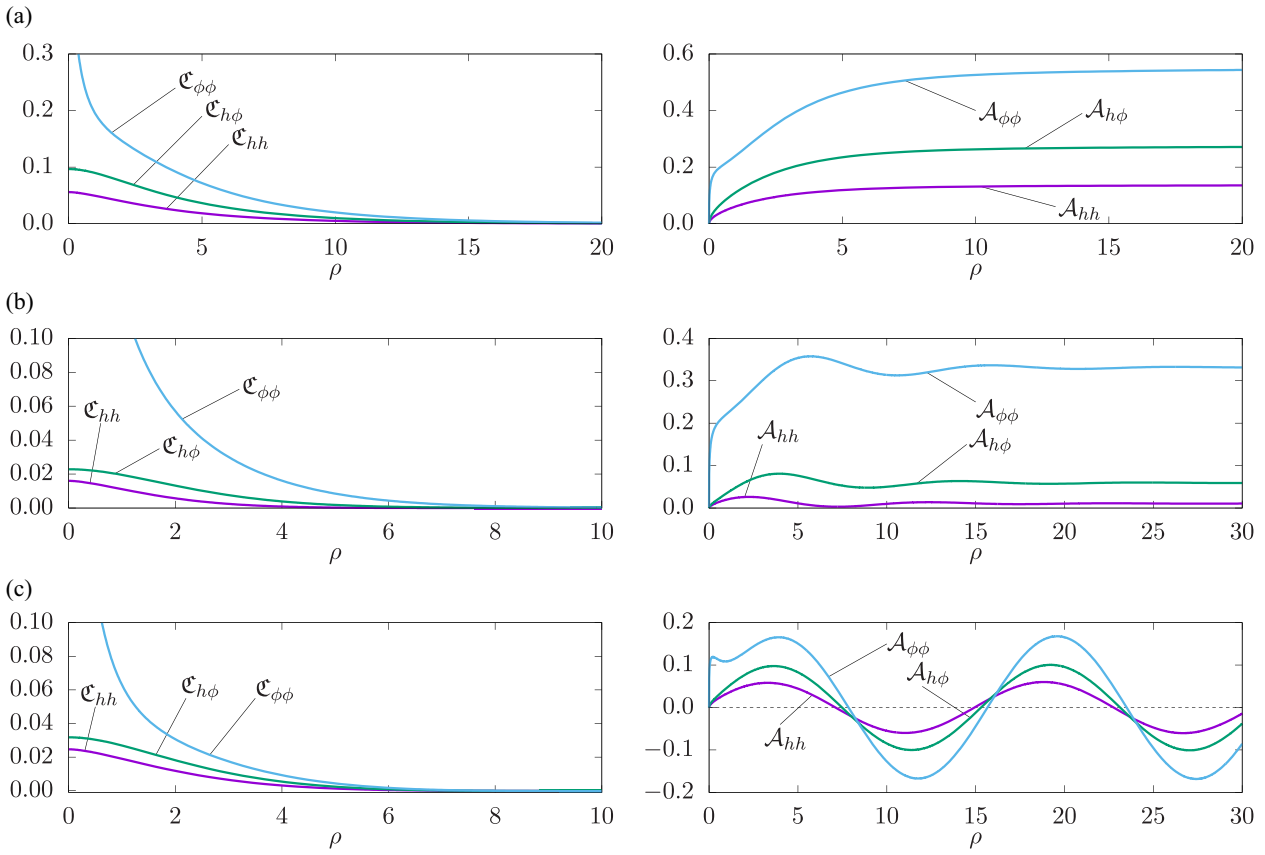

FIG. 3. Example plots of the correlation functions $\mathfrak{C}_{hh}$, $\mathfrak{C}_{h\phi}$, and $\mathfrak{C}_{\phi\phi}$, and their amplitudes in different zones as functions of the distance ρ. (a) $\kappa = 10$, $\tau = 0.02$, and $\mu = 0.5$ (zone I), (b) $\kappa = 10$, $\tau = 0.15$, and $\mu = 0.2$ (zone II), (c) $\kappa = 10$, $\tau = 0.30$, and $\mu = 0.5$ (zone III). The values of parameters used here have been marked with blue dots in Fig. 2. In each panel the plot on the left presents the correlation functions, and the plot on the right their amplitudes [see Eq. (16)]. The behavior of the amplitudes is different in each zone.

function of ρ. Only when $1/t_2$ is much smaller than ξ might the amplitude stay monotonic, but the oscillations are still visible. Finally, in zone III, where the oscillating term dominates, the amplitude has no limit for $\rho \to \infty$. Instead, it oscillates around zero. For large ρ these oscillations have period $\mathfrak{P} = 2\pi/a$, and for smaller ρ higher order terms perturb slightly the amplitudes. The full correlation functions [see (16)] decay to zero exponentially in zones I and II and like a damped oscillation in zone III.

The correlation functions, upon crossing the border of zones, show a smooth crossover between different asymptotic behaviors. Typically, two different length scales become comparable or the period of oscillations diverges. This means that, close to the border, the size of the system necessary to observe characteristic behavior of the correlation functions becomes very large. We have not observed any phase transition associated with changing of the zones. Detailed analysis of the observed crossover is beyond the scope of this paper.

The plots of the correlation functions and their amplitudes in different zones are presented in Fig. 3.

The phenomenon of different asymptotics of the correlation function is well known in the literature in the context of the theory of fluids; the line separating regions with exponential and damped oscillatory decay of the correlation functions (in our case borderline between zone III and other zones) is called the Fisher-Widom line [53,69,70]. We note that, even though the mathematical mechanism generating the Fisher-Widom line is the same, its physical reason is different. While in fluids the oscillations appear due to layering of particles, in our model the oscillations are the result of minimizing the energy of an elastic membrane.

E. Correlation length

In this subsection we discuss the properties of the correlation length $\xi(\tau, \omega)$ given by Eq. (17) that describes the exponential decay of all the correlation functions.

Even though the correlation length ξ has been defined separately in each of the zones, it is a continuous function of its parameters; upon crossing the border between zone I or II and zone III the derivative $\partial\xi/\partial\tau$ is discontinues and can even be divergent. On the contrary, there is no nonanalyticity associated with crossing the border between zones I and II, which is in line with the properties of the roots of the polynomial; see Fig. 7(b) below. We stress that the nonanalyticity appears only in the correlation length; it is not present in the correlation functions.

For large values of the reduced temperature τ,

$$\xi(\tau, \omega) = \sqrt{2} + O(1/\tau), \quad \text{for } \tau \to \infty. \tag{18}$$

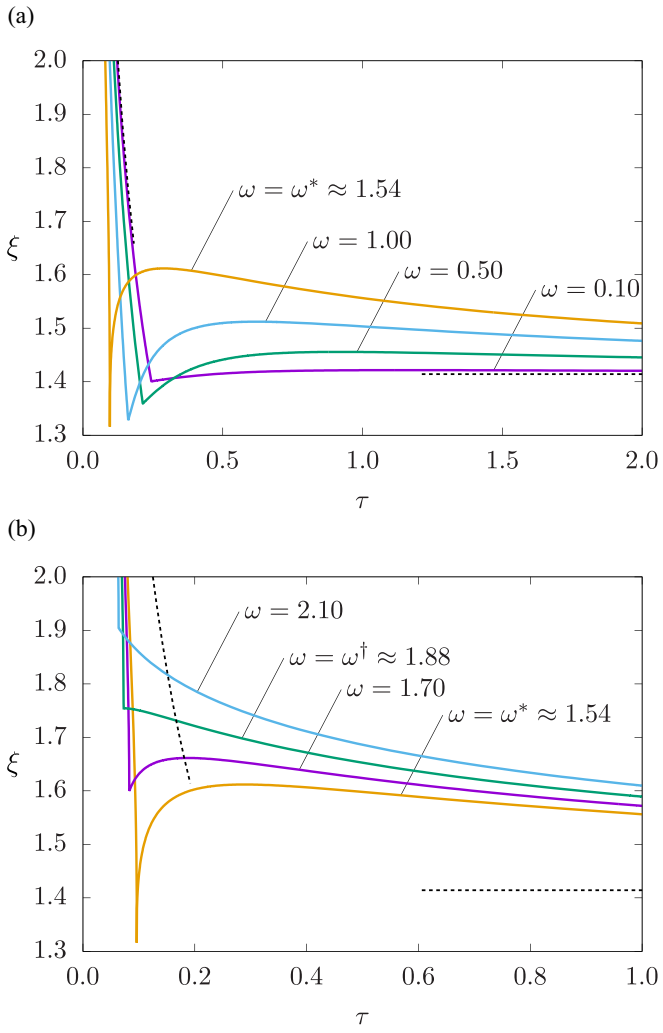

FIG. 4. Correlation length ξ as a function of τ for different values of ω. (a) For $\omega < \omega^*$ the minimum gets deeper upon increasing ω; (b) for $\omega > \omega^*$ the value in the minimum increases upon increasing ω and, eventually, disappears for $\omega = \omega^\dagger$. The dashed lines denote the asymptotic behavior of the correlation length (which is independent of ω): $(2\tau)^{-1/2}$ for small τ, and $\sqrt{2}$ for large τ. The kinks, visible for all the curves, are associated with crossing the border between two different zones: in (a) from zone II for small τ to zone III for large τ, and in (b) from zone I to zone III. Crossing from zone I to zone II is not associated with any nonanalyticity of ξ, and for the selected values of ω it is located beyond the range of the plot.

This result agrees with the correlation length [measured in units ζ; see (5)] reported for a membrane without the composition order parameter $\phi(\boldsymbol{\rho})$ [66]. This limit is discussed in Appendix E 1.

When the reduced temperature is close to zero, we have

$$\xi(\tau, \omega) = (2\tau)^{-1/2} + O(\tau^{1/2}), \tag{19}$$

which means that for $\tau \to 0$ our model becomes critical and ξ diverges with the critical exponent $\nu = 1/2$. This value is characteristic for the Gaussian model. The properties of the correlation functions in this limit are presented in Appendix E 2.

In Fig. 4 we present the plots of the correlation length ξ as a function of τ for several fixed values of ω. When ω is small, for small τ the correlation function is a decreasing function of τ and has a minimum exactly when the parameters are on the border between zones II and III (see Fig. 2). For this special value of τ, ξ is nonanalytic and the derivative $\partial\xi/\partial\tau$ jumps from a finite negative value to a finite positive value. For larger values of τ the correlation length, upon increasing τ, first increases, has a shallow maximum, and decreases to the asymptotic value $\sqrt{2}$. Upon increasing ω [for small values of ω, see Fig. 4(a)] the shape of the correlation function plotted as a function of τ changes only slightly. The value of τ for which there is a minimum is slowly decreasing (following the border between zones II and III) and gets deeper. At the same time the jump of the derivative $\partial\xi/\partial\tau$ in the minimum is increasing, and the value in the minimum is decreasing.

The above picture changes when, upon increasing ω, $\omega = \omega^* = 8/(3\sqrt{3}) \approx 1.54$ is reached, i.e., the value in the point where all three zones meet. In the minimum [observed for $\tau = \tau^* = 1/(6\sqrt{3}) \approx 0.0962$] the derivative $\partial\xi/\partial\tau$ is $-\infty$ from the left side and $+\infty$ from the right side. In this special point the correlation function has the smallest possible value

$$\xi_{\min} = \xi(\tau^*, \omega^*) = 3^{1/4} \approx 1.32 \quad \text{(in units of } \zeta\text{)}. \tag{20}$$

Upon further increasing of ω [see Fig. 4(b)], the minimum moves towards smaller values of τ, following the border between zones I and III. The derivative $\partial\xi/\partial\tau$ stays (minus) infinite from the left side, but the right side derivative is finite and decreasing. For $\omega = \omega^\dagger = \frac{4}{5}(10 - 2\sqrt{5})^{1/2} \approx 1.88$ the right side derivative changes its sign; for $\omega \geqslant \omega^\dagger$ the correlation length ξ does not have a minimum, and, as a function of τ, it monotonically decreases. At the border between zone I and III there is still a point of nonanalyticity with an infinite left side derivative $\partial\xi/\partial\tau$.

These properties of the correlation length ξ can potentially be used to experimentally estimate the value of ω and, thus, the coupling between order parameters α. The value of τ for which ξ is nonanalytic and (for $\omega < \omega^\dagger$) has a minimum is uniquely related to the value of ω.

F. Period of oscillations

Another quantity that can potentially be measured experimentally is the period of oscillations of the correlation function. The oscillations are visible only in zones II and III, and their period is

$$\mathfrak{P} = \frac{2\pi}{a}, \tag{21}$$

where a is determined by the roots of polynomial (11) (it is the real part of the complex root). This period can be reliably estimated from the plot of the correlation function only when $\mathfrak{P}/\xi \ll 1$; otherwise the exponential decay damps the oscillations too fast, like is illustrated in Fig. 3(c).

As we have checked numerically, in zone III for large τ the period $\mathfrak{P} = 2\pi\sqrt{2}$, while the correlation length $\xi = \sqrt{2}$ (in units of ζ), which gives $\mathfrak{P}/\xi = 2\pi$. Upon decreasing τ both the period and the correlation length are growing but the ratio $\mathfrak{P}/\xi$ is increasing, making it harder to measure the period of oscillations. Finally, upon approaching the border of the zone, the period reaches a finite value for the border between zones III and II, or infinity for the border between zones III and I.

The situation is different in zone II, where the oscillations do not dominate for large distances, but they are still visible on top of exponentially decaying correlation function. In this case, the ratio $\mathfrak{P}/\xi$ can be small, especially for $\tau \to 0$, where the correlation length diverges while the period of oscillations stays finite. Nevertheless, in this zone the decay of oscillations is governed by a length scale $\xi_1 = 1/t_2$, which is smaller than the correlation length. As we have checked numerically, in zone II the ratio $\mathfrak{P}/\xi_1$ is always larger than 2π.

To conclude, for all possible values of parameters, the decay of oscillations has a length scale comparable to the period of oscillations and, therefore, experimental measuring of it must be very challenging, if possible at all.

G. Correlation functions in different limiting cases

We conclude the analysis of the correlation functions in the model by studying their behavior in various limiting cases. In order to keep the text compact, the detailed analysis is reported in Appendix E; here we provide only the most important results.

When the reduced temperature is big ($\tau \to \infty$ limit and ℓ_ϕ much smaller than other length scales) the composition order parameter ϕ becomes negligible, and thus the correlation functions $\mathfrak{C}_{\phi\phi}$ and $\mathfrak{C}_{h\phi}$ go to zero. In this limit only the order parameter h is relevant and the results known for the membrane deformation model are recovered.

When, on the other hand, the reduced temperature is small ($\tau \to 0$ limit and $\ell_\phi \gg \ell_h, \ell_{\text{coupling}}$) the system becomes critical and all the correlation functions are proportional to a single scaling function, the same as in the Gaussian model. Surprisingly, only the formula for $\mathfrak{C}_{\phi\phi}$ is strictly universal; the other correlation functions still depend on the parameter μ describing the strength of the coupling.

In the case of weak coupling between order parameters ($\mu \to 0$ limit and ℓ_{coupling} much larger than other scales) the correlation function $\mathfrak{C}_{h\phi}$ is vanishing. Surprisingly, the two order parameters stay coupled for a nonzero μ and decay with the same correlation length. Only when $\mu = 0$ does the decay for $\mathfrak{C}_{hh}$ and $\mathfrak{C}_{\phi\phi}$ happen on different length scales.

When the coupling between the order parameters is strong ($\mu \to \infty$ and $\ell_{\text{coupling}} \ll \ell_h, \ell_\phi$) the correlation length diverges and the system is again critical. We identify this limit with critical roughening present in the membrane deformation model without external potential. All the correlation functions can be described with a single scaling function.

We have also considered a limit of $\gamma \to \infty$ in the coupling term in the Hamiltonian (3), which implies $\ell_{\text{coupling}} \ll \ell_h \ll \ell_\phi$. As we show in Appendix E 5, it is equivalent to the limit of both $\tau \to 0$ and $\mu \to \infty$ with $\tau\mu^2$ fixed. Even though any of these limits alone imply criticality, when they are applied together the system in not critical anymore. In fact, it can be mapped to a membrane deformation model with both elastic and surface energy included.

IV. ORDER PARAMETER PROFILES AND SIZE OF INDUCED DOMAINS

Now we introduce a single anchor into the membrane, i.e., we put $N = 1$ in Eq. (6), and discuss the resulting order parameter profiles. For simplicity, we assume that the inclusion is located in the origin ($\boldsymbol{\rho}_1 = \mathbf{0}$), and thus the system has a rotational symmetry with respect to the origin. As a result, the equilibrium values of the order parameters depend on the distance from the origin ρ and not on the exact position $\boldsymbol{\rho}$. In Appendix B 2, using the method based on path integrals, we show that

$$\langle h(\rho)\rangle = h_1 \mathfrak{C}_{hh}(\rho;\kappa,\tau,\mu)/\mathfrak{C}_{hh}(0;\kappa,\tau,\mu), \tag{22a}$$

$$\langle \phi(\rho)\rangle = h_1 \mathfrak{C}_{h\phi}(\rho;\kappa,\tau,\mu)/\mathfrak{C}_{hh}(0;\kappa,\tau,\mu), \tag{22b}$$

where h_1 denotes the value of the order parameter h imposed on the membrane in the pinning point $\boldsymbol{\rho}_1 = \mathbf{0}$. Depending on the interpretation of h, this can be either fixed excess thickness that matches the hydrophobic mismatch of the anchoring protein or fixed position of the membrane imposed by the anchor attached to the cytoskeleton. The formulas for the order parameter profiles $\langle h(\rho)\rangle$ and $\langle \phi(\rho)\rangle$ are equal to properly rescaled correlation functions $\mathfrak{C}_{hh}$ and $\mathfrak{C}_{h\phi}$, respectively. This implies that the order parameters have a different asymptotic behavior in the three zones identified in Sec. III.

Here we skip the detailed analysis of $\langle h(\rho)\rangle$ and $\langle \phi(\rho)\rangle$ in different regimes as this would only repeat the discussion of the correlation functions presented in Sec. III. Moreover, the plots of the profiles in different zones have already been presented in [31].

When the excess thickness of the membrane is fixed to some nonzero value in the origin, the order parameter $h(\boldsymbol{\rho})$ is also nonzero in the region surrounding the pinning point, and, due to the coupling between order parameters, $\phi(\boldsymbol{\rho})$ also is nonzero there. Of course, the farther away from the origin we go, the smaller the magnitudes of the order parameters are. We identify the perturbation in the order parameters caused by the presence of the anchor with experimentally observed so-called domains of lipids that form around the pinning points [31,39]. In order to facilitate the comparison between our model and experimental systems, it is necessary to introduce an effective size $\mathfrak{R}$ of the induced domain. We note that in our model, the membrane is always above the critical temperature, where there is only a single bulk phase (with equilibrium average of both order parameters equal zero); therefore the observed perturbations cannot be the domains in the strict sense of the meaning. This explains why there is no straightforward, unique definition of the radius of such a domain. In this section we discuss six possible ways to define such a quantity (three different definitions applied to two order parameters).

A. Effective radii based on integrated order parameters

We define the excess adsorption Γ_{ex} and the excess volume V_{ex} via

$$\Gamma_{\text{ex}}(\kappa,\mu,\tau,h_1) = 2\pi \int_0^\infty \langle \phi(\rho)\rangle \rho \, d\rho, \tag{23a}$$

$$V_{\text{ex}}(\kappa,\mu,\tau,h_1) = 2\pi \int_0^\infty \langle h(\rho)\rangle \rho \, d\rho, \tag{23b}$$

i.e., the area integral of the composition and thickness order parameter profiles. Excess adsorption is proportional to the additional amount of the component of the membrane preferred by the anchor that has gathered around it, and excess

volume is equal to the additional volume (measured in ζ^3 unit) of the membrane due to the hydrophobic mismatch of the anchor. We note that both quantities can be positive or negative: the sign of ϕ, and hence $\Gamma_{\rm ex}$, determines the type of lipids that the anchor effectively prefers, whereas positive (negative) $V_{\rm ex}$ corresponds to the hydrophobic core of the anchor larger (smaller) than the preferred distance between the leaflets of an unperturbed membrane. Using Eq. (22), after some algebra, we get

$$\Gamma_{\rm ex}(\kappa,\mu,\tau,h_1)=\frac{h_1\mu}{2\tau\mathfrak{C}_{h\phi}(0;\kappa,\tau,\mu)}, \tag{24a}$$

$$V_{\rm ex}(\kappa,\mu,\tau,h_1)=\frac{h_1(2\tau+\kappa\mu^2)}{2\tau\kappa\mathfrak{C}_{hh}(0;\kappa,\tau,\mu)}. \tag{24b}$$

Both quantities are continuous functions of all their parameters, and they are linear in the thickness of the membrane h_1 imposed by the inclusion. For small τ they have a divergence of a type $(\tau\ln\tau)^{-1}$. For $\tau\to\infty$, the excess adsorption $\Gamma_{\rm ex}$ decays to zero like τ^{-1}, while the excess volume $V_{\rm ex}$ has a finite limit $8h_1$.

From definition (23a) and Eq. (22b) it follows that, upon approaching the critical point, the excess adsorption is determined by the integral of the mixed correlation function $\mathfrak{C}_{h\phi}$. We recall that for systems described by a single order parameter, the integral of the (dimensionless) correlation function is equal to the susceptibility and diverges as $\sim|t|^{-\gamma}$, where $t=(T-T_{\rm c})/T_{\rm c}$ is the reduced temperature and γ is the critical exponent [21]. For the Gaussian model $\gamma=1$ and logarithmic correction are expected, and $\tau\sim t$; hence our results are in agreement with this general law. Moreover, the same law applies to $V_{\rm ex}$ which is based on the order parameter h, which shows that, due to the coupling, in the limit $\tau\to 0$ the critical behavior is relevant for both order parameters, as we have observed in Appendix E 2.

The excess adsorption can be used to define the effective size of the induced domain. For a given set of parameters κ, μ, τ, and h_1, we consider a simplified circular deformation of the membrane of the radius $\mathfrak{R}_\Gamma$ with a constant chemical composition inside equal to $\langle\phi(0)\rangle$, a zero composition order parameter outside, and the same excess adsorption as the real deformation. Using (24a) we get

$$\mathfrak{R}_\Gamma(\kappa,\mu,\tau)=\left(\frac{\mu}{2\pi\tau\,\mathfrak{C}_{hh}(0;\kappa,\tau,\mu)}\right)^{1/2}. \tag{25a}$$

Similarly, one can define the effective radius $\mathfrak{R}_V$ as the radius of the circular deformation of fixed thickness h_1 and the same volume as the real deformation:

$$\mathfrak{R}_V(\kappa,\mu,\tau)=\left(\frac{2\tau+\kappa\mu^2}{2\pi\tau\kappa\,\mathfrak{C}_{hh}(0;\kappa,\tau,\mu)}\right)^{1/2}. \tag{25b}$$

B. Effective radii based on local properties of the order parameters

Another possible definitions of the effective radius are based on local properties of the order parameters. When observing the thickness of the membrane or its chemical composition it is natural to place the border of the deformation in the place where the observed quantity is changing in the fastest way, i.e., where the derivative is the biggest—in the inflection point. Therefore, we introduce two effective radii $\mathfrak{R}^\phi_{\rm infl}$ and $\mathfrak{R}^h_{\rm infl}$ based on the inflection points:

$$\frac{\partial^2}{\partial\rho^2}\langle\phi(\rho)\rangle\Big|_{\rho=\mathfrak{R}^\phi_{\rm infl}(\kappa,\mu,\tau)}=0, \tag{25c}$$

$$\frac{\partial^2}{\partial\rho^2}\langle h(\rho)\rangle\Big|_{\rho=\mathfrak{R}^h_{\rm infl}(\kappa,\mu,\tau)}=0, \tag{25d}$$

where, in the case of zone III, one has to take the smallest positive ρ fulfilling the above condition. Unlike $\mathfrak{R}_\Gamma$ and $\mathfrak{R}_V$, these two radii are based on local properties of the order parameter, which makes their analytical analysis more challenging.

Finally, the effective size of the domain can be defined as a distance at which the magnitude of the order parameter reaches half of its value in the center of the domain

$$\left\langle\phi\left(\mathfrak{R}^\phi_{1/2}(\kappa,\mu,\tau)\right)\right\rangle=\tfrac{1}{2}\langle\phi(0)\rangle, \tag{25e}$$

$$\left\langle h\left(\mathfrak{R}^h_{1/2}(\kappa,\mu,\tau)\right)\right\rangle=\tfrac{1}{2}\langle h(0)\rangle. \tag{25f}$$

This definition is especially handful when working with microscope images of experimental system.

We note that all six radii introduced here do not depend on the thickness h_1 of the membrane set by an inclusion. For $\mathfrak{R}_\Gamma$ and $\mathfrak{R}_V$ changing of h_1 is changing the reference value of the relevant order parameter at $\boldsymbol{\rho}=\mathbf{0}$ together with the excess adsorption and the excess volume, and for $\mathfrak{R}^\phi_{\rm infl}$, $\mathfrak{R}^h_{\rm infl}$, $\mathfrak{R}^\phi_{1/2}$, and $\mathfrak{R}^h_{1/2}$ varying h_1 changes the magnitude of the order parameters but does not shift the inflection point or the midpoint.

C. Comparison of effective radii in different limiting cases

We have calculated rigorously the asymptotic behavior of all the radii for large and small values of their parameters—the results are summarized in Table II.

For $\tau\to 0$ the values of $\mathfrak{R}_\Gamma$ and $\mathfrak{R}_V$ diverge in exactly the same, independent of the value of $\omega=\kappa\mu^2$ way $\sim|\tau\ln\tau|^{1/2}$. The divergence is slower than the divergence of the correlation length $\xi\sim\tau^{-1/2}$ only by a logarithmic factor; this seems to be a manifestation of the universality principle. The radii $\mathfrak{R}^\phi_{1/2}$ and $\mathfrak{R}^h_{1/2}$ also diverge for $\tau\to 0$ but like $\tau^{-1/4}$, i.e., much slower than ξ, $\mathfrak{R}_\Gamma$, and $\mathfrak{R}_V$, and with ω-dependent amplitude. In contrast, radii $\mathfrak{R}^\phi_{\rm infl}$ and $\mathfrak{R}^h_{\rm infl}$ in the limit $\tau\to 0$ approach two different, finite, ω-dependent values. We note that, for $\tau=0$ our model is not well defined, and therefore these limiting values cannot be reached. These results imply that for small values of τ,

$$\xi\gg\mathfrak{R}_\Gamma>\mathfrak{R}_V\gg\mathfrak{R}^\phi_{1/2}>\mathfrak{R}^h_{1/2}\gg\mathfrak{R}^\phi_{\rm infl}>\mathfrak{R}^h_{\rm infl},\quad\text{for }\tau\to 0. \tag{26}$$

The example behavior of the radii for small τ is presented in Figs. 5(a) and 5(b).

In the limit $\tau\to\infty$ all radii approach finite, nonzero, ω-independent values. In this limit

$$\mathfrak{R}_\Gamma\gtrapprox\mathfrak{R}_V\gtrapprox\sqrt{8/\pi}>\xi\gtrapprox\sqrt{2}>\mathfrak{R}^\phi_{1/2}\gtrapprox\mathfrak{R}^h_{1/2}\gtrapprox\mathfrak{R}^\dagger>\mathfrak{R}^\phi_{\rm infl}\gtrapprox\mathfrak{R}^h_{\rm infl}\gtrapprox\mathfrak{R}^*,\quad\text{for }\tau\to\infty, \tag{27}$$

TABLE II. Asymptotic behavior of six effective radii for small and large effective temperature τ and the coupling constant μ (the bending stiffness κ is assumed to be constant). Only leading order terms in a given limit are given; the limits $\tau \to 0, \infty$ are calculated for fixed μ, and the limits $\mu \to 0, \infty$ are for fixed τ. The special values $\mathfrak{R}^*$ and $\mathfrak{R}^\dagger$ are defined in Eq. (28).

Radius	Definition of effective radius	$\tau \to 0$	$\tau \to \infty$	$\mu \to 0$	$\mu \to \infty$
$\mathfrak{R}_\Gamma$	Excess adsorption	$\sqrt{2}\lvert\tau \ln \tau\rvert^{-1/2}$	$\sqrt{8/\pi} \approx 1.596$	τ-dependent constant	$\sqrt{8/\pi}\,[\kappa\mu^2/(2\tau)]^{1/4}$
$\mathfrak{R}_V$	Excess volume	$\sqrt{2}\lvert\tau \ln \tau\rvert^{-1/2}$	$\sqrt{8/\pi} \approx 1.596$	$\sqrt{8/\pi} \approx 1.596$	$\sqrt{8/\pi}\,[\kappa\mu^2/(2\tau)]^{1/4}$
$\mathfrak{R}^\phi_{\text{infl}}$	Inflection point of $\langle\phi\rangle$	ω-dependent constant	$\mathfrak{R}^* \approx 0.8096$	τ-dependent constant	$\mathfrak{R}^*[\kappa\mu^2/(2\tau)]^{1/4}$
$\mathfrak{R}^h_{\text{infl}}$	Inflection point of $\langle h\rangle$	ω-dependent constant	$\mathfrak{R}^* \approx 0.8096$	$\mathfrak{R}^* \approx 0.8096$	$\mathfrak{R}^*[\kappa\mu^2/(2\tau)]^{1/4}$
$\mathfrak{R}^\phi_{1/2}$	Half of maximal value of $\langle\phi\rangle$	$f_1(\omega)\tau^{-1/4}$	$\mathfrak{R}^\dagger \approx 1.302$	τ-dependent constant	$\mathfrak{R}^\dagger[\kappa\mu^2/(2\tau)]^{1/4}$
$\mathfrak{R}^h_{1/2}$	Half of maximal value of $\langle h\rangle$	$f_2(\omega)\tau^{-1/4}$	$\mathfrak{R}^\dagger \approx 1.302$	$\mathfrak{R}^\dagger \approx 1.302$	$\mathfrak{R}^\dagger[\kappa\mu^2/(2\tau)]^{1/4}$

where

$$\text{kei}(\mathfrak{R}^\dagger) = \frac{1}{2}\,\text{kei}\,(0), \quad \mathfrak{R}^\dagger \approx 1.302, \tag{28a}$$

$$\frac{d^2}{d\rho^2}\,\text{kei}\,(\rho)\bigg|_{\rho=\mathfrak{R}^*} = 0, \quad \mathfrak{R}^* \approx 0.8096 \tag{28b}$$

[where $\mathfrak{R}^*$ is the smallest positive solution of (28b)]. The behavior of radii for large τ is illustrated in Figs. 5(a) and 5(b).

When $\mu \to 0$ (which for fixed κ is equivalent to $\omega \to 0$) all radii approach finite values. For radii based on chemical composition ϕ, this limit depends on τ, while for radii based on h it does not depend on any parameter; see Table II. As presented in Fig. 5(c), upon reducing μ, depending on the values of other parameters, the relation between the radii can change.

Finally, in the limit $\mu \to \infty$ all radii are proportional to $[\kappa\mu^2/(2\tau)]^{1/4} \sim \mu^{1/2}$. In this limit (like in the case of large values of τ), we observe that the radii group into pairs that become asymptotically equal:

$$\begin{aligned}
&\mathfrak{R}_\Gamma, \mathfrak{R}_V \approx \sqrt{8/\pi}\left(\frac{\kappa\mu^2}{2\tau}\right)^{1/4} > \xi \approx \sqrt{2}\left(\frac{\kappa\mu^2}{2\tau}\right)^{1/4} \\
&> \mathfrak{R}^\phi_{1/2}, \mathfrak{R}^h_{1/2} \approx \mathfrak{R}^\dagger\left(\frac{\kappa\mu^2}{2\tau}\right)^{1/4} \\
&> \mathfrak{R}^\phi_{\text{infl}}, \mathfrak{R}^h_{\text{infl}} \approx \mathfrak{R}^*\left(\frac{\kappa\mu^2}{2\tau}\right)^{1/4}, \quad \text{for } \mu \to \infty,
\end{aligned} \tag{29}$$

where we have used Eq. (E13). The above behavior of the radii has been illustrated in Fig. 5(c). Surprisingly, the amplitudes multiplying the dominant divergence $[\kappa\mu^2/(2\tau)]^{1/4}$ are identical to the limiting values of the radii for $\tau \to \infty$. We also note that, depending on the radius and parameters, the asymptotic formula can be approached both from below and from above (which is in contrast with the limit $\tau \to \infty$, where the limiting value was always approached from above).

The above rigorous analysis has been supported by numerical calculation of all the radii. We have not noted any nonanalytical behavior of the radii upon crossing the borders of the three regimes discussed in Sec. III, which is different from the behavior of ξ. In zone III all the radii are of the same order as the correlation length ξ, while in zones I and II, in the limit $\tau \to 0$, the radii and the correlation length can be significantly different [cf. Eq. (26)]. For all tested values of parameters, we have observed that all radii are decreasing upon increasing τ, and they are increasing upon increasing μ. We have also checked that

$$\begin{aligned}
&\mathfrak{R}_\Gamma > \mathfrak{R}_V > \sqrt{8/\pi}, \quad \mathfrak{R}^\phi_{1/2} > \mathfrak{R}^h_{1/2} > \mathfrak{R}^\dagger, \\
&\text{and} \quad \mathfrak{R}^\phi_{\text{infl}} > \mathfrak{R}^h_{\text{infl}} > \mathfrak{R}^*,
\end{aligned} \tag{30}$$

where $\mathfrak{R}^\dagger$ and $\mathfrak{R}^*$ are defined in Eq. (28). For most of the tested values of parameters we have also observed $\mathfrak{R}_V > \mathfrak{R}^\phi_{1/2}$ and $\mathfrak{R}^h_{1/2} > \mathfrak{R}^\phi_{\text{infl}}$; however, when both τ and μ are small this relation does not hold.

Finally we note that each of $\mathfrak{R}_V$, $\mathfrak{R}^h_{1/2}$, and $\mathfrak{R}^h_{\text{infl}}$ has the same limiting value for $\tau \to \infty$ and for $\mu \to 0$ (equal, respectively, to $\sqrt{8/\pi}$, $\mathfrak{R}^\dagger$, and $\mathfrak{R}^*$). Closer investigation shows that for small values of μ these functions are almost constant, except for a small region around $\tau = 0$, for which their value is significantly higher. Upon reducing μ the size of this region is decreasing. Such a behavior suggests the existence of a scaling limit for $\mu \to 0$ and $\tau \to 0$. The detailed analysis of the model in this limit and the discussion of the physical relevance of the membrane with strongly fluctuating composition order parameter weakly coupled to spatial degrees of freedom go beyond the scope of this paper.

V. DISCUSSION

The main goal of this paper was to investigate the structure properties of a simple model that couples the composition of the two-component lipid membrane to a membrane shape order parameter that describes two different situations: deformations of the local thickness of the membrane or deformations of its local position. This coupling is relevant in the context of domain formation in cell membranes and model membranes. For example, it has been observed that membrane lipids segregate near anchors linking the membrane to the cytoskeletal actin filaments. Typically, these anchors have a hydrophobic part with a thickness slightly different from that of the hydrophobic part of the membrane. Due to this hydrophobic mismatch, the hydrophobic core of the membrane locally deforms, effectively attracting to this region lipids with an appropriate length of the hydrophobic acyl chain. The same mechanism would apply whenever proteins or anchors have a hydrophobic part with a thickness slightly different from that of the hydrophobic part of the membrane. Another possible mechanism for creating lipid domains around proteins is by deforming the membranes through ligand-receptor

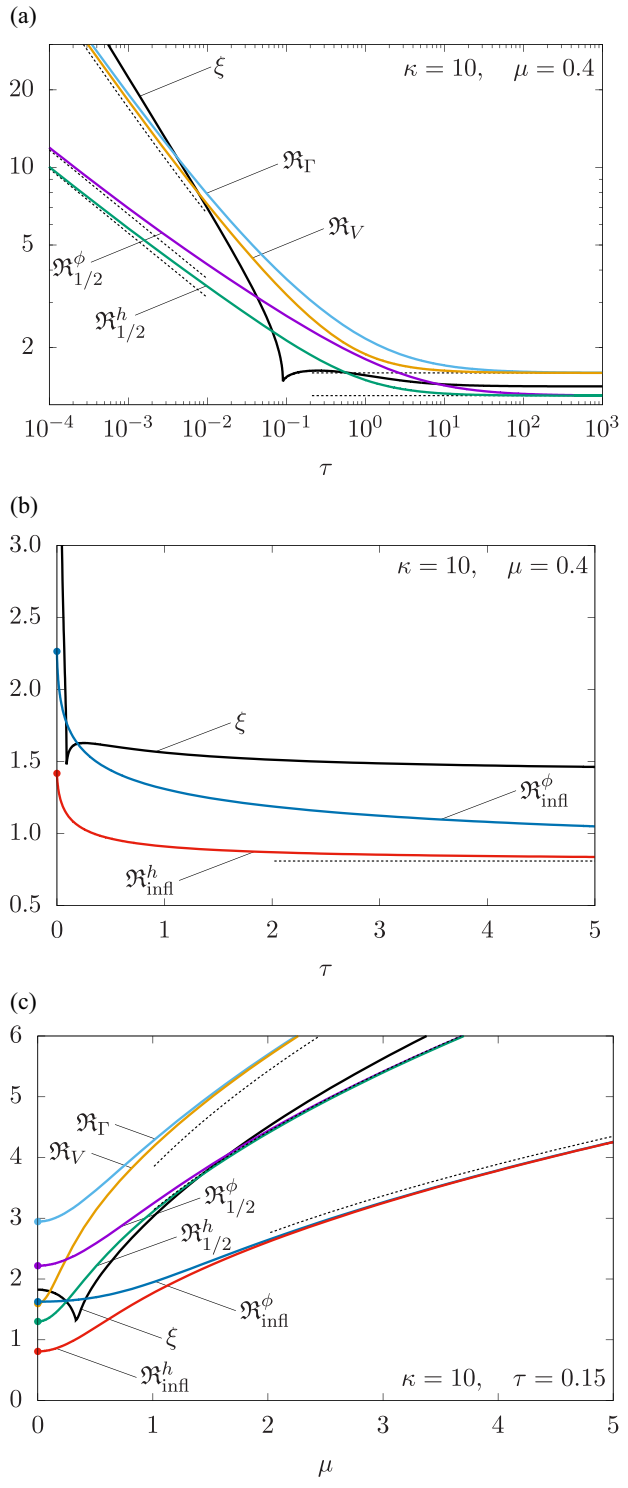

FIG. 5. Plots of the effective radii $\mathfrak{R}_\Gamma$, $\mathfrak{R}_V$, $\mathfrak{R}^\phi_{\text{infl}}$, $\mathfrak{R}^h_{\text{infl}}$, $\mathfrak{R}^\phi_{1/2}$, and $\mathfrak{R}^h_{1/2}$ describing the size of the domain induced by the defect. (a), (b) Plot of six radii as functions of τ for $\kappa = 10$ and $\mu = 0.4$. (c) Plot of the radii as a function of μ for fixed $\kappa = 10$ and $\tau = 0.15$. In all panels, the dashed lines denote the asymptotic behavior for τ, $\mu \to 0, \infty$, and the dots for $\tau = 0$ and $\mu = 0$ denote the finite limits of the radii; cf. Table II.

interactions with the structures in the extracellular space. In this case the composition of the membrane can be affected by the change of the average separation from the opposing, adherent surface, namely, the displacement of the membrane may result in the expulsion of the proteins of the glycocalyx from the region of the contact. Likewise, a significant redistribution of charged moieties may take place. In both cases the nonspecific interactions of the adherent membrane will be affected, which can drive modification of the membrane composition. Such a process is responsible for protein organization during the formation of the T-cell synapse or natural killer cell activation. The same scenario has been observed in integrin or cadherin adhesion.

The advantage of our model is that it can be solved exactly. Using the path integral approach, we have calculated analytically correlation functions of all three pairs of order parameters. Our model has three independent (dimensionless) parameters. One of them, i.e., the reduced deviation from the critical temperature of membrane demixing τ, is a natural control parameter in experiments. The parameter describing membrane elasticity κ can in principle be measured. This is not the case for the third parameter, which is the strength of coupling between the local deformation of the membrane thickness (or the membrane height) and the local change in the lipid concentration μ. However, as we argued in Sec. III E, its value can be estimated from the behavior of the correlation length, which is measurable.

In the phase space spanned by these parameters we have distinguished three zones of distinct functional forms of the two-point correlation functions. In all zones the leading asymptotic decay is exponential; however, it is multiplied by different prefactors: in zones I and II by a constant number, and by an oscillating function in zone III. Close to the critical point, in zones I and II this behavior is very similar to the one observed in the Landau-Ginzburg model, whereas away from criticality, in zone III it resembles the membrane deformation model behavior.

These correlations are responsible for enhanced concentration order parameter near an inclusion embedded in the membrane, which locally change the thickness (height) of a membrane. This phenomenon is an analog of critical adsorption occurring in binary liquid mixtures upon approaching critical point of demixing from a homogeneous phase. We have found that excess adsorption of membrane lipids of one kind diverges in the same way as predicted for two-dimensional Ising-like systems near symmetry-breaking pointlike inclusions [21]. In order to facilitate comparisons with experiments, we have proposed several definitions of the size of domains rich in the lipid effectively attracted to the inclusion, and we have discussed their universal aspects, advantages, and disadvantages. For example, for a study of coalescence of two domains in comparison with images from microscope, it is convenient to use $\mathfrak{R}^\phi_{1/2}$. However, like for all other proposed radii, this definition does not depend on the hydrophobic mismatch of the inclusion, so the size of the domain is not changing upon increasing the mismatch, which is counterintuitive.

The current work has several very natural extensions. First, one can include the ϕ^4 term in the Hamiltonian. This allows for studying the model at and below the critical temperature but requires numerical calculations. Second, one can introduce several inclusions in arrangement that mimics anchors linking the membrane to the actin network, and compare the

lipid concentration field with experimental images. Due to the presence of quenched disorder along the lines following the filaments of the actin, such a model can be treated only numerically. Third, one can also add to our model a coupling between the curvature of a membrane and its composition, and study the combine effect of the two mechanisms of domain formation. Finally, this model can also be used to study membrane-mediated Casimir-like interactions between floating inclusions. These effective forces could be very strong and might be a dominant factor in the process of formation of clusters of proteins on the membrane.

ACKNOWLEDGMENTS

The authors thank P. Jakubczyk, M. Napiórkowski, and A. Parry for inspiring discussions and suggestions. The paper has been supported by the German Research Foundation and the French National Research Agency project SM 289/8-1, AOBJ: 652939/ANR-18-CE92-0033-01, and by German Research Foundation project SM 289/10-1. A.M. was partially supported by the Polish National Science Center (Opus Grant No. 2022/45/B/ST3/00936).

APPENDIX A: EFFECT OF THE SURFACE TENSION OF THE MEMBRANE

In this Appendix we discuss how the properties of our model change when nonzero surface tension η is considered; see Eq. (1). In such a case, the part of the dimensionless Hamiltonian $\beta\mathcal{H}_{\rm MD}$ giving the energy associated with the shape of the membrane [cf. Eq (6b)] is

$$\beta\mathcal{H}_{\rm MD} = \int d\boldsymbol{\rho}\left(\frac{\kappa}{2}[\nabla^2 h(\boldsymbol{\rho})]^2 + \frac{\kappa\vartheta}{2}[\nabla h(\boldsymbol{\rho})]^2\right), \tag{A1}$$

where $\vartheta = \eta/(\kappa\gamma)^{1/2}$ is the dimensionless variable proportional to the surface tension η of the membrane.

Using the path integral method, we have calculated the formulas for the correlation functions for the extended Hamiltonian

$$\mathfrak{C}_{hh}(\rho;\kappa,\tau,\mu,\vartheta) = \frac{1}{2\pi\kappa}\int_0^\infty \frac{x(x^2+\omega+2\tau)\mathcal{J}_0(\rho x)}{(x^4+\vartheta x^2+1)(x^2+2\tau+\omega)-\omega}\,dx, \tag{A2a}$$

$$\mathfrak{C}_{h\phi}(\rho;\kappa,\tau,\mu,\vartheta) = \frac{\mu}{2\pi}\int_0^\infty \frac{x\,\mathcal{J}_0(\rho x)}{(x^4+\vartheta x^2+1)(x^2+2\tau+\omega)-\omega}\,dx, \tag{A2b}$$

$$\mathfrak{C}_{\phi\phi}(\rho;\kappa,\tau,\mu,\vartheta) = \frac{1}{2\pi}\int_0^\infty \frac{x(x^4+\vartheta x^2+1)\mathcal{J}_0(\rho x)}{(x^4+\vartheta x^2+1)(x^2+2\tau+\omega)-\omega}\,dx, \tag{A2c}$$

which is equivalent to Eq. (A2) with x^4+1 replaced with $x^4+\vartheta x^2+1$ [and, of course, it reduces to (A2) for $\vartheta=0$].

The calculation of the integrals (A2) can be done in exactly the same way as for the original integrals. Again, the properties of the correlation functions depend on the roots of the polynomial in the denominator

$$\tilde{W}(z;\omega,\tau,\vartheta) = (z^4+\vartheta z^2+1)(z^2+2\tau+\omega)-\omega. \tag{A3}$$

The properties of the roots split the space of parameters (ω,τ) into three distinct zones whose shape now depends on ϑ. In zone I all six roots are imaginary $\pm it_1$, $\pm it_2$, and $\pm it_3$ with $t_1<t_2<t_3$. In zones II and III there are two imaginary roots $\pm it_1$ and four complex roots $\pm a\pm it_2$, and $t_1<t_2$ in zone II while $t_1>t_2$ in zone III. The correlation functions $\mathfrak{C}_{hh}$ and $\mathfrak{C}_{h\phi}$ are given by exactly the same formulas (12) and (15) as in the case of a membrane without a surface tension, but the parameters t_1, t_2, t_3, and a are now given by the roots of the polynomial (A3). The situation is slightly different in the case of $\mathfrak{C}_{\phi\phi}$ since ϑ appears in the nominator of the integrand (A2c); after a short calculation we get the following: in zone I,

$$\mathfrak{C}_{\phi\phi}(\rho;\kappa,\tau,\mu,\vartheta) = \frac{1}{2\pi}\left[\frac{\mathcal{K}_0(\rho t_1)\left(t_1^4-\vartheta t_1^2+1\right)}{\left(t_1^2-t_2^2\right)\left(t_1^2-t_3^2\right)} + \frac{\mathcal{K}_0(\rho t_2)\left(t_2^4-\vartheta t_2^2+1\right)}{\left(t_2^2-t_1^2\right)\left(t_2^2-t_3^2\right)} + \frac{\mathcal{K}_0(\rho t_3)\left(t_3^4-\vartheta t_3^2+1\right)}{\left(t_3^2-t_1^2\right)\left(t_3^2-t_2^2\right)}\right], \tag{A4a}$$

and in zones II and III,

$$\mathfrak{C}_{\phi\phi}(\rho;\kappa,\tau,\mu,\vartheta) = \frac{1}{2\pi}\left[\frac{\mathcal{K}_0(\rho t_1)\left(t_1^4-\vartheta t_1^2+1\right)}{\left(t_1^2-t_2^2\right)^2+2a^2\left(t_1^2+t_2^2\right)+a^4} - \mathrm{Im}\left(\frac{\mathcal{K}_0[\rho(t_2+ia)][(a-it_2)^4+\vartheta(a-it_2)^2+1]}{2at_2\left[t_1^2+(a-it_2)^2\right]}\right)\right]. \tag{A4b}$$

The dependence of the zone diagram on the value of the reduced surface tension ϑ is presented in Fig. 6. For $\vartheta=0$ we recover the diagram for the model without surface tension; see Fig. 2. Upon increasing ϑ, zone III is decreasing, and zones I and II are increasing. This is especially visible for larger values of ω. As we have checked, the line between the I and III approaches for large ω an asymptote

$$\tau_{\rm I/III}^{\rm asymptote}(\omega;\vartheta) = \frac{\vartheta^2}{8-2\vartheta^2}\,\omega + \frac{\vartheta}{4}, \text{ for large } \omega. \tag{A5}$$

The situation changes when, upon increasing ϑ, the value $\vartheta=2$ is reached [see Fig. 6(f)]. Starting from that point zone III completely disappears, and the space of parameters is split only into two zones. Upon further increasing of ϑ zone II is slowly growing, and the line between the zones approaches

$$\tau_{\rm I/II}^{\rm asymptote}(\omega;\vartheta) = -\frac{\vartheta}{4+2\vartheta}\,\omega + \frac{\vartheta}{2}, \text{ for large } \vartheta, \tag{A6}$$

with some deviations for very small ω. A similar behavior has been reported in the model without a composition order parameter [53]: upon increasing the surface tension of the membrane, at some point the order parameter stops showing oscillations.

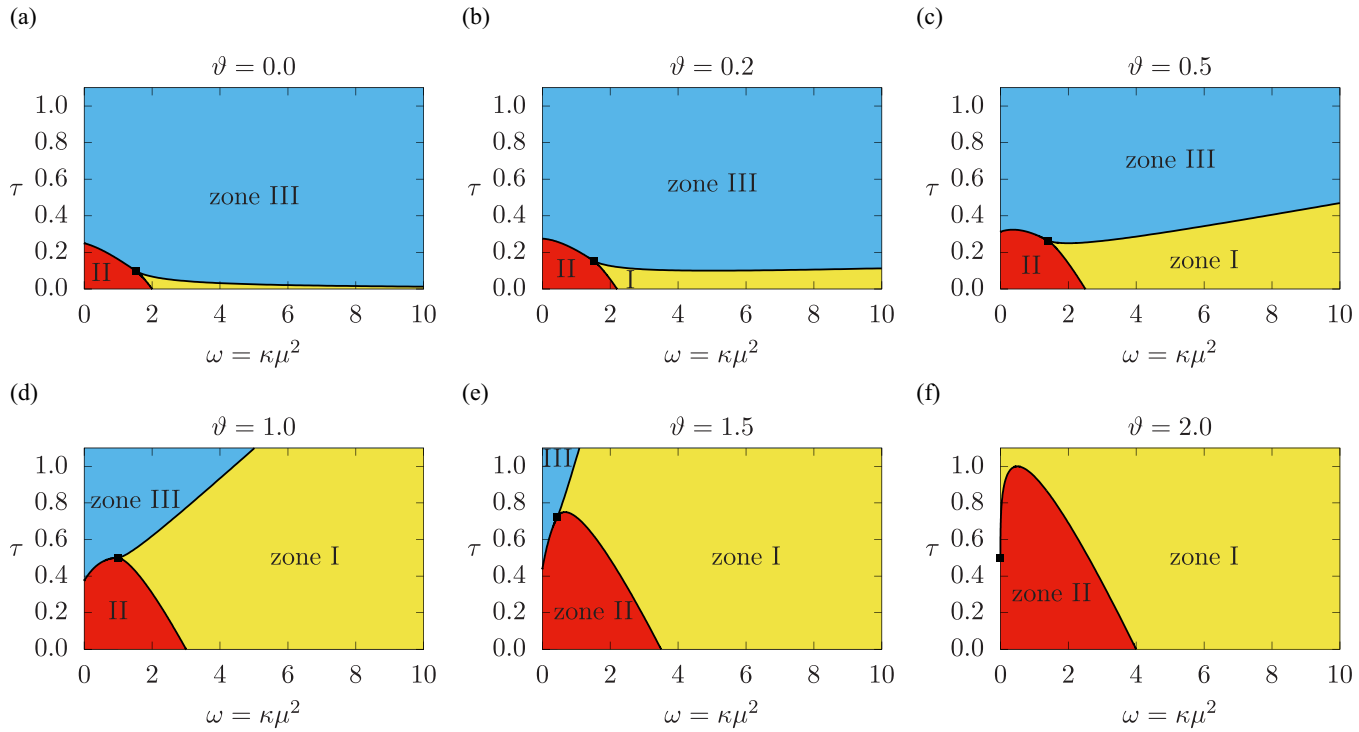

FIG. 6. Schematic plot presenting how the three zones are changed by the surface tension η of the membrane. (a) $\vartheta = \eta/(\kappa\gamma)^{1/2} = 0$, (b) $\vartheta = 0.2$, (c) $\vartheta = 0.5$, (d) $\vartheta = 1.0$, (e) $\vartheta = 1.5$, and (f) $\vartheta = 2$. On every plot the black square marks the point where all three zones meet. The color code used to denote the zones is the same in every panel.

We have also checked numerically that for $\vartheta < 2$ the correlation length is the smallest in the point where all three zones meet (denoted by a black square in Fig. 6). Moreover, for $\vartheta > 0$ this minimal value is larger than $3^{1/4}$, the minimal value of the correlation length in a model without surface tension η [see Eq. (20)].

We conclude that introducing nonzero surface tension of the membrane, as long as $\vartheta = \eta/(\kappa\gamma)^{1/2} < 2$, is changing the system only quantitatively; the main qualitative properties remain unchanged.

Finally we note that introducing nonzero η is changing the behavior of our system in some limiting cases. In the limit $\mu \to \infty$ ($\ell_{\text{coupling}} \ll \ell_h, \ell_\phi$), while for $\vartheta = 0$ the system is in zone III, it is in zone I for $\vartheta > 0$. In the limit $\gamma \to \infty$ (cf. App. E 5) the reduced temperature t is effectively shifted by a term proportional to η.

APPENDIX B: METHOD OF CALCULATIONS

In this Appendix we present the details of the calculation of the formulas used in the paper. The calculation is based on [66], where the membrane with a single order parameter $h(\boldsymbol{r})$ is studied. We have decided to include the derivations here because the additional order parameter $\phi(\boldsymbol{r})$, described by the Hamiltonian of the Gaussian model, makes it necessary to regularize the integrals by introducing the cutoff, which was not necessary in [66].

1. Correlation functions

To calculate the correlation functions for the membrane without pinning points we calculate the probability density of having $h(\boldsymbol{\rho}_\mathrm{a}) = h_\mathrm{a}$, $\phi(\boldsymbol{\rho}_\mathrm{a}) = \phi_\mathrm{a}$, $h(\boldsymbol{\rho}_\mathrm{b}) = h_\mathrm{b}$, and $\phi(\boldsymbol{\rho}_\mathrm{b}) = \phi_\mathrm{b}$. In a canonical ensemble it is given by

$$\begin{aligned}\mathfrak{p}(\boldsymbol{\rho}_\mathrm{a}, h_\mathrm{a}, \phi_\mathrm{a}, \boldsymbol{\rho}_\mathrm{b}, h_\mathrm{b}, \phi_\mathrm{b}; \kappa, \mu, \tau) \\ = \text{const} \int \mathcal{D}h(\boldsymbol{\rho}) \int \mathcal{D}\phi(\boldsymbol{\rho}) \delta[h(\boldsymbol{\rho}_\mathrm{a}) - h_\mathrm{a}]\delta[\phi(\boldsymbol{\rho}_\mathrm{a}) - \phi_\mathrm{a}]\delta[h(\boldsymbol{\rho}_\mathrm{b}) - h_\mathrm{b}]\delta[\phi(\boldsymbol{\rho}_\mathrm{b}) - \phi_\mathrm{b}] \exp\{-\beta\mathcal{H}[h(\boldsymbol{\rho}), \phi(\boldsymbol{\rho})]\},\end{aligned} \tag{B1}$$

where the term const denotes a constant prefactor (its exact value is not relevant, the final value is determined using the normalization condition), $\int \mathcal{D}h(\boldsymbol{\rho}) \int \mathcal{D}\phi(\boldsymbol{\rho})$ is the path integral over all possible configurations of the two order parameters, δ denotes the Dirac delta function (it is used to fix the values of the order parameters in $\boldsymbol{\rho}_\mathrm{a}$ and $\boldsymbol{\rho}_\mathrm{b}$), and the Hamiltonian $\beta\mathcal{H}$ is given by Eq. (6) without the pinning part ($N = 0$).

Using the relation

$$\delta(x) = \frac{1}{2\pi} \int_{-\infty}^{\infty} d\psi\, e^{i\psi x}, \tag{B2}$$

we transform Eq. (B1) into

$$\mathfrak{p}(\boldsymbol{\rho}_\mathrm{a}, h_\mathrm{a}, \phi_\mathrm{a}, \boldsymbol{\rho}_\mathrm{b}, h_\mathrm{b}, \phi_\mathrm{b}; \kappa, \mu, \tau) = \mathrm{const} \int \mathcal{D}h(\boldsymbol{\rho}) \int \mathcal{D}\phi(\boldsymbol{\rho}) \int_{-\infty}^{\infty} d\psi_1 \int_{-\infty}^{\infty} d\psi_2 \int_{-\infty}^{\infty} d\psi_3 \int_{-\infty}^{\infty} d\psi_4 \exp\{-\beta\mathcal{H}[h(\boldsymbol{\rho}), \phi(\boldsymbol{\rho})] + i\psi_1 h(\boldsymbol{\rho}_\mathrm{a}) + i\psi_2\phi(\boldsymbol{\rho}_\mathrm{a}) + i\psi_3 h(\boldsymbol{\rho}_\mathrm{b}) + i\psi_4\phi(\boldsymbol{\rho}_\mathrm{b}) - i\psi_1 h_\mathrm{a} - i\psi_2\phi_\mathrm{a} - i\psi_3 h_\mathrm{b} - i\psi_4\phi_\mathrm{b}\}. \quad \text{(B3)}$$

The next step is to introduce the Fourier transform of the order parameters

$$h(\boldsymbol{\rho}) = \sum_{|\boldsymbol{q}|<\Lambda} h_{\boldsymbol{q}} e^{i\boldsymbol{q}\boldsymbol{\rho}}, \quad \phi(\boldsymbol{\rho}) = \sum_{|\boldsymbol{q}|<\Lambda} \phi_{\boldsymbol{q}} e^{i\boldsymbol{q}\boldsymbol{\rho}}, \quad \text{(B4)}$$

where, in order to regularize some prefactors and integrals, we have introduced a cutoff Λ; to obtain the final results we apply the limit $\Lambda \to \infty$. The allowed values of the wave vector $\boldsymbol{q}$, assuming square shape of the membrane of the area A and periodic boundary conditions, are

$$\boldsymbol{q} = \frac{2\pi}{\sqrt{A}}(n, m), \quad n, m \in \mathbb{Z}, \quad |\boldsymbol{q}| < \Lambda. \quad \text{(B5)}$$

Using (B4) we transform all the terms of Hamiltonian (6). After some algebra we get

$$\beta\mathcal{H}_\mathrm{MD} = A \sum_{|\boldsymbol{q}|<\Lambda} \frac{\kappa}{2} q^4 |h_{\boldsymbol{q}}|^2, \quad \text{(B6a)}$$

$$\beta\mathcal{H}_\mathrm{G} = A \sum_{|\boldsymbol{q}|<\Lambda} \left(\frac{1}{2}q^2 + \tau\right) |\phi_{\boldsymbol{q}}|^2, \quad \text{(B6b)}$$

$$\beta\mathcal{H}_\mathrm{C} = A \sum_{|\boldsymbol{q}|<\Lambda} \frac{\kappa}{2} (|h_{\boldsymbol{q}}|^2 + \mu^2 |\phi_{\boldsymbol{q}}|^2 - 2\mu h_{\boldsymbol{q}} \phi_{\boldsymbol{q}}^*), \quad \text{(B6c)}$$

where we have used identities $h_{-\boldsymbol{q}} = h_{\boldsymbol{q}}^*$ and $\phi_{-\boldsymbol{q}} = \phi_{\boldsymbol{q}}^*$ which follow from the fact that the order parameters $h(\boldsymbol{\rho})$ and $\phi(\boldsymbol{\rho})$ are real-valued functions. Using the above result in Eq. (B3), after some reordering of terms in the exponent we get

$$\mathfrak{p}(\boldsymbol{\rho}_\mathrm{a}, h_\mathrm{a}, \phi_\mathrm{a}, \boldsymbol{\rho}_\mathrm{b}, h_\mathrm{b}, \phi_\mathrm{b}; \kappa, \mu, \tau) = \mathrm{const} \int \mathcal{D}h(\boldsymbol{\rho}) \int \mathcal{D}\phi(\boldsymbol{\rho}) \int_{-\infty}^{\infty} d\psi_1 \int_{-\infty}^{\infty} d\psi_2 \int_{-\infty}^{\infty} d\psi_3 \int_{-\infty}^{\infty} d\psi_4 \exp\Bigg\{ - \sum_{|\boldsymbol{q}|<\Lambda} \Bigg[A\frac{\kappa}{2}(q^4+1)|h_{\boldsymbol{q}}|^2 + \frac{A}{2}(q^2 + 2\tau + \omega)|\phi_{\boldsymbol{q}}|^2 - A\kappa\mu h_{\boldsymbol{q}}\phi_{\boldsymbol{q}}^* - i\psi_1 h_{\boldsymbol{q}} e^{i\boldsymbol{q}\boldsymbol{\rho}_\mathrm{a}} - i\psi_2\phi_{\boldsymbol{q}} e^{i\boldsymbol{q}\boldsymbol{\rho}_\mathrm{a}} - i\psi_3 h_{\boldsymbol{q}} e^{i\boldsymbol{q}\boldsymbol{\rho}_\mathrm{b}} - i\psi_4\phi_{\boldsymbol{q}} e^{i\boldsymbol{q}\boldsymbol{\rho}_\mathrm{b}} \Bigg] - i\psi_1 h_\mathrm{a} - i\psi_2\phi_\mathrm{a} - i\psi_3 h_\mathrm{b} - i\psi_4\phi_\mathrm{b} \Bigg\}. \quad \text{(B7)}$$

In order to simplify the above formula it is necessary to define what exactly is meant by the path integral $\int \mathcal{D}x(\boldsymbol{\rho})$, where x denotes one of the order parameters h or ϕ. Clearly, one has to integrate over all degrees of freedom $x_{\boldsymbol{q}}$ describing the function $x(\boldsymbol{\rho})$, but they are not independent variables since $x_{-\boldsymbol{q}} = x_{\boldsymbol{q}}^*$. Therefore, we group together all terms containing $x_{\boldsymbol{q}}$ and $x_{-\boldsymbol{q}}$, and integrate them separately over real and imaginary part of $x_{\boldsymbol{q}}$. Since

$$\int_{-\infty}^{\infty} d\,\mathrm{Re}\, x_{\boldsymbol{q}} \int_{-\infty}^{\infty} d\,\mathrm{Im}\, x_{\boldsymbol{q}} e^{-a(\boldsymbol{q})|x_{\boldsymbol{q}}|^2 - 2b(\boldsymbol{q})x_{\boldsymbol{q}}} e^{-a(-\boldsymbol{q})|x_{-\boldsymbol{q}}|^2 - 2b(-\boldsymbol{q})x_{-\boldsymbol{q}}} = \left[\sqrt{\frac{\pi}{2a(\boldsymbol{q})}} \exp\left(\frac{b(\boldsymbol{q})b(-\boldsymbol{q})}{a(\boldsymbol{q})}\right)\right]^2 \quad \text{(B8a)}$$

and

$$\int_{-\infty}^{\infty} dx_{\boldsymbol{0}}\, e^{-a(\boldsymbol{0})|x_{\boldsymbol{0}}|^2 - 2b(\boldsymbol{0})x_{\boldsymbol{0}}} = \sqrt{\frac{\pi}{a(\boldsymbol{0})}} \exp\left(\frac{b(\boldsymbol{0})^2}{a(\boldsymbol{0})}\right), \quad \text{(B8b)}$$

where we have used the fact that $x_{\boldsymbol{0}}$ is real and assumed that $a(-\boldsymbol{q}) = a(\boldsymbol{q})$; we can use the following rule for calculating the path integrals:

$$\int \mathcal{D}x(\boldsymbol{\rho}) \exp\left\{ - \sum_{|\boldsymbol{q}|<\Lambda} [a(\boldsymbol{q})|x_{\boldsymbol{q}}|^2 + 2b(\boldsymbol{q})x_{\boldsymbol{q}}] \right\} = \mathrm{const} \exp\left[\sum_{|\boldsymbol{q}|<\Lambda} \frac{b(\boldsymbol{q})b(-\boldsymbol{q})}{a(\boldsymbol{q})} \right]. \quad \text{(B9)}$$

We note that the omitted constant depends on the parameters present in $a(\boldsymbol{q})$, which in our case are κ, μ, and τ. The strict calculation of the constant standing in front of the integral for the probability $\mathfrak{p}$ requires including not only all the prefactors from Eq. (B8) but also a Jacobian coming from the change of variables made with the Fourier transform. Moreover, such a constant is clearly cutoff dependent and may diverge in the limit $\Lambda \to \infty$ or $A \to \infty$. Here we avoid all these problems by calculating the constant via the normalization of the probability distribution.

Applying the transformation (B9) for $h(\boldsymbol{\rho})$ in Eq. (B7) with

$$a(\boldsymbol{q}) = \frac{A\kappa}{2}(q^4+1), \tag{B10a}$$

$$2b(\boldsymbol{q}) = -A\kappa\mu\phi^*_{\boldsymbol{q}} - i\psi_1 e^{i\boldsymbol{q}\boldsymbol{\rho}_\mathrm{a}} - i\psi_3 e^{i\boldsymbol{q}\boldsymbol{\rho}_\mathrm{b}}, \tag{B10b}$$

after a short derivation gives

$$\begin{aligned}
&\mathfrak{p}(\boldsymbol{\rho}_\mathrm{a}, h_\mathrm{a}, \phi_\mathrm{a}, \boldsymbol{\rho}_\mathrm{b}, h_\mathrm{b}, \phi_\mathrm{b}; \kappa, \mu, \tau) \\
&= \mathrm{const}\int \mathcal{D}\phi(\boldsymbol{\rho}) \int_{-\infty}^{\infty} d\psi_1 \int_{-\infty}^{\infty} d\psi_2 \int_{-\infty}^{\infty} d\psi_3 \int_{-\infty}^{\infty} d\psi_4 \exp\Bigg\{ -\sum_{|\boldsymbol{q}|<\Lambda} \Bigg[\frac{A}{2} \frac{(q^4+1)(q^2+2\tau+\omega)-\omega}{q^4+1} |\phi_{\boldsymbol{q}}|^2 \\
&+ \frac{\psi_1^2+\psi_3^2}{2A\kappa(q^4+1)} - \frac{i\,\mu}{q^4+1} e^{i\boldsymbol{q}\boldsymbol{\rho}_\mathrm{a}} \psi_1 \phi_{\boldsymbol{q}} - \frac{i\,\mu}{q^4+1} e^{i\boldsymbol{q}\boldsymbol{\rho}_\mathrm{b}} \psi_3 \phi_{\boldsymbol{q}} + \frac{\cos \boldsymbol{q}(\boldsymbol{\rho}_\mathrm{a}-\boldsymbol{\rho}_\mathrm{b})}{A\kappa(q^4+1)} \psi_1\psi_3 \\
&- i\psi_2\phi_{\boldsymbol{q}} e^{i\boldsymbol{q}\boldsymbol{\rho}_\mathrm{a}} - i\psi_4\phi_{\boldsymbol{q}} e^{i\boldsymbol{q}\boldsymbol{\rho}_\mathrm{b}} \Bigg] - i\psi_1 h_\mathrm{a} - i\psi_2\phi_\mathrm{a} - i\psi_3 h_\mathrm{b} - i\psi_4\phi_\mathrm{b} \Bigg\}.
\end{aligned} \tag{B11}$$

In the resulting formula one of the factors has the exact form of the polynomial from Eq. (11): $W(q) = (q^4+1)(q^2+2\tau+\omega) - \omega$. The transformation (B9) can now be applied to Eq. (B11) in order to calculate the path integral over $\phi(\boldsymbol{\rho})$. From Eq. (B11) we read

$$a(\boldsymbol{q}) = \frac{A}{2}\frac{W(q)}{q^4+1}, \tag{B12a}$$

$$2b(\boldsymbol{q}) = -\frac{i\,\mu}{q^4+1} e^{i\boldsymbol{q}\boldsymbol{\rho}_\mathrm{a}} \psi_1 - \frac{i\,\mu}{q^4+1} e^{i\boldsymbol{q}\boldsymbol{\rho}_\mathrm{b}} \psi_3 - i\psi_2 e^{i\boldsymbol{q}\boldsymbol{\rho}_\mathrm{a}} - i\psi_4 e^{i\boldsymbol{q}\boldsymbol{\rho}_\mathrm{b}}. \tag{B12b}$$

After some algebra we derive

$$\begin{aligned}
&\mathfrak{p}(\boldsymbol{\rho}_\mathrm{a}, h_\mathrm{a}, \phi_\mathrm{a}, \boldsymbol{\rho}_\mathrm{b}, h_\mathrm{b}, \phi_\mathrm{b}; \kappa, \mu, \tau) \\
&= \mathrm{const}\int_{-\infty}^{\infty} d\psi_1 \int_{-\infty}^{\infty} d\psi_2 \int_{-\infty}^{\infty} d\psi_3 \int_{-\infty}^{\infty} d\psi_4 \exp\Bigg\{ -\frac{1}{A}\sum_{|\boldsymbol{q}|<\Lambda} \Bigg[\frac{q^2+2\tau+\omega}{2\kappa W(q)} \left(\psi_1^2+\psi_3^2\right) \\
&+ \frac{q^4+1}{2W(q)} \left(\psi_2^2+\psi_4^2\right) + \frac{\mu}{W(q)} (\psi_1\psi_2+\psi_3\psi_4) + \frac{\mu\cos \boldsymbol{q}(\boldsymbol{\rho}_\mathrm{a}-\boldsymbol{\rho}_\mathrm{b})}{W(q)} (\psi_1\psi_4+\psi_2\psi_3) \\
&+ \frac{(q^2+2\tau+\omega)\cos \boldsymbol{q}(\boldsymbol{\rho}_\mathrm{a}-\boldsymbol{\rho}_\mathrm{b})}{\kappa W(q)} \psi_1\psi_3 + \frac{(q^4+1)\cos \boldsymbol{q}(\boldsymbol{\rho}_\mathrm{a}-\boldsymbol{\rho}_\mathrm{b})}{W(q)} \psi_2\psi_4 \Bigg] - i\psi_1 h_\mathrm{a} - i\psi_2\phi_\mathrm{a} - i\psi_3 h_\mathrm{b} - i\psi_4\phi_\mathrm{b} \Bigg\}.
\end{aligned} \tag{B13}$$

To simplify the above formula it is convenient to take the limit $A \to \infty$. From Eq. (B5) it follows that, upon increasing A, the allowed values of $\boldsymbol{q}$ are getting closer to each other, and in the limit of infinite area, the sum is replaced with an integral following a formula

$$\lim_{A\to\infty} \frac{1}{A} \sum_{|\boldsymbol{q}|<\Lambda} f(\boldsymbol{q}) = \frac{1}{4\pi^2} \int_{|\boldsymbol{q}|<\Lambda} d\boldsymbol{q} f(\boldsymbol{q}), \tag{B14}$$

valid for any function $f(\boldsymbol{q})$ that decays sufficiently fast for large q.

We introduce three functions:

$$\begin{aligned}
\bar{\mathfrak{C}}_{hh}(\rho_\mathrm{ab}) &= \frac{1}{4\pi^2} \int_{|\boldsymbol{q}|<\Lambda} d\boldsymbol{q} \frac{(q^2+2\tau+\omega)\cos \boldsymbol{q}(\boldsymbol{\rho}_\mathrm{a}-\boldsymbol{\rho}_\mathrm{b})}{\kappa W(q)} \\
&= \frac{1}{2\pi\kappa} \int_0^{\Lambda} dq \frac{q(q^2+2\tau+\omega)\mathcal{J}_0(q\rho_\mathrm{ab})}{W(q)},
\end{aligned} \tag{B15a}$$

$$\begin{aligned}
\bar{\mathfrak{C}}_{h\phi}(\rho_\mathrm{ab}) &= \frac{1}{4\pi^2} \int_{|\boldsymbol{q}|<\Lambda} d\boldsymbol{q} \frac{\mu\cos \boldsymbol{q}(\boldsymbol{\rho}_\mathrm{a}-\boldsymbol{\rho}_\mathrm{b})}{W(q)} \\
&= \frac{\mu}{2\pi} \int_0^{\Lambda} dq \frac{q\mathcal{J}_0(q\rho_\mathrm{ab})}{W(q)},
\end{aligned} \tag{B15b}$$

$$\begin{aligned}
\bar{\mathfrak{C}}_{\phi\phi}(\rho_\mathrm{ab}) &= \frac{1}{4\pi^2} \int_{|\boldsymbol{q}|<\Lambda} d\boldsymbol{q} \frac{(q^4+1)\cos \boldsymbol{q}(\boldsymbol{\rho}_\mathrm{a}-\boldsymbol{\rho}_\mathrm{b})}{W(q)} \\
&= \frac{1}{2\pi} \int_0^{\Lambda} dq \frac{q(q^4+1)\mathcal{J}_0(q\rho_\mathrm{ab})}{W(q)},
\end{aligned} \tag{B15c}$$

where we have defined $\rho_{ab} = |\boldsymbol{\rho}_a - \boldsymbol{\rho}_b|$, and simplified the integrals by performing the integral over the direction of vector $\boldsymbol{q}$. We note that the functions have been given a bar to distinguish them from the correlation functions [see Eq. (10)]. Our goal in this subsection is to prove that, in the limit $\Lambda \to \infty$, they are actually equal to the correlation functions.

Using Eq. (B15), formula for the probability in Eq. (B13) can be written in the form

$$\begin{aligned}\mathfrak{p}(\boldsymbol{\rho}_a, h_a, \phi_a, \boldsymbol{\rho}_b, h_b, \phi_b; \kappa, \mu, \tau) = \text{const} \int_{-\infty}^{\infty} d\psi_1 \int_{-\infty}^{\infty} d\psi_2 \int_{-\infty}^{\infty} d\psi_3 \int_{-\infty}^{\infty} d\psi_4 \exp\Big[-\frac{1}{2}\bar{\mathfrak{C}}_{hh}(0)\big(\psi_1^2+\psi_3^2\big) - \frac{1}{2}\bar{\mathfrak{C}}_{\phi\phi}(0)\big(\psi_2^2+\psi_4^2\big) \\ - \bar{\mathfrak{C}}_{h\phi}(0)(\psi_1\psi_2 + \psi_3\psi_4) - \bar{\mathfrak{C}}_{h\phi}(\rho_{ab})(\psi_1\psi_4 + \psi_2\psi_3) - \bar{\mathfrak{C}}_{hh}(\rho_{ab})\psi_1\psi_3 - \bar{\mathfrak{C}}_{\phi\phi}(\rho_{ab})\psi_2\psi_4 \\ - i\psi_1 h_a - i\psi_2\phi_a - i\psi_3 h_b - i\psi_4\phi_b\Big]. \end{aligned} \tag{B16}$$

We note that the coefficient $\bar{\mathfrak{C}}_{\phi\phi}(0)$ diverges for $\Lambda \to \infty$. This is the main motivation for introducing the regularization.

Using the matrix notation, the formula in Eq. (B16) for the probability can be rewritten in a form

$$\begin{aligned}&\mathfrak{p}(\boldsymbol{\rho}_a, h_a, \phi_a, \boldsymbol{\rho}_b, h_b, \phi_b; \kappa, \mu, \tau) \\ &\quad = \text{const} \int d\boldsymbol{\Psi} \exp\left(-\frac{1}{2}\boldsymbol{\Psi}^{\mathrm{T}}\mathbb{M}\boldsymbol{\Psi} - i\boldsymbol{\Phi}^{\mathrm{T}}\boldsymbol{\Psi}\right),\end{aligned} \tag{B17}$$

where the four-dimensional vector $\boldsymbol{\Psi} = [\psi_1, \psi_2, \psi_3, \psi_4]^{\mathrm{T}}$, $\boldsymbol{\Phi} = [h_a, \phi_a, h_b, \phi_b]^{\mathrm{T}}$, the symbol "T" denotes transposition of the vector or matrix, and the symmetric matrix $\mathbb{M}$ is given by

$$\mathbb{M} = \begin{bmatrix} \bar{\mathfrak{C}}_{hh}(0) & \bar{\mathfrak{C}}_{h\phi}(0) & \bar{\mathfrak{C}}_{hh}(\rho_{ab}) & \bar{\mathfrak{C}}_{h\phi}(\rho_{ab}) \\ \bar{\mathfrak{C}}_{h\phi}(0) & \bar{\mathfrak{C}}_{\phi\phi}(0) & \bar{\mathfrak{C}}_{h\phi}(\rho_{ab}) & \bar{\mathfrak{C}}_{\phi\phi}(\rho_{ab}) \\ \bar{\mathfrak{C}}_{hh}(\rho_{ab}) & \bar{\mathfrak{C}}_{h\phi}(\rho_{ab}) & \bar{\mathfrak{C}}_{hh}(0) & \bar{\mathfrak{C}}_{h\phi}(0) \\ \bar{\mathfrak{C}}_{h\phi}(\rho_{ab}) & \bar{\mathfrak{C}}_{\phi\phi}(\rho_{ab}) & \bar{\mathfrak{C}}_{h\phi}(0) & \bar{\mathfrak{C}}_{\phi\phi}(0) \end{bmatrix}. \tag{B18}$$

This reveals the simple structure of the formula for the probability in Eq. (B17). We have imposed four conditions on the membrane: (1) in point $\boldsymbol{\rho}_a$ the order parameter h is equal to h_a, (2) in point $\boldsymbol{\rho}_a$ the order parameter ϕ is equal to ϕ_a, (3) in point $\boldsymbol{\rho}_b$ the order parameter h is equal to h_b, and finally, (4) in point $\boldsymbol{\rho}_b$ the order parameter ϕ is equal to h_b. The element of the matrix $\mathbb{M}_{ij}$ is solely related to the conditions i and j. The type of the correlation function is selected based on the fields that are fixed, and the argument of the correlation function is the distance between the points where the conditions are imposed. The second term in the exponent in Eq. (B17) sets the relation between variables ψ_i and the values of fixed order parameters for the four conditions imposed on the membrane. We note that this rule can easily be extended to an arbitrary number of points where the order parameters are fixed and, therefore, allows one to skip the part of the calculations with path integrals. We leave the mathematical proof of correctness of this general procedure as a simple exercise.

The integral in Eq. (B17) can be calculated using the matrix analog of Eq. (B8),

$$\begin{aligned}&\int d\boldsymbol{v} \exp\left(-\frac{1}{2}\boldsymbol{v}^{\mathrm{T}}\mathbb{A}\boldsymbol{v} + \boldsymbol{w}^{\mathrm{T}}\boldsymbol{v}\right) \\ &\quad = \frac{(2\pi)^{n/2}}{\sqrt{\det \mathbb{A}}} \exp\left(\frac{1}{2}\boldsymbol{w}^{\mathrm{T}}\mathbb{A}^{-1}\boldsymbol{w}\right),\end{aligned} \tag{B19}$$

where $\mathbb{A}$ is an arbitrary, $n \times n$, symmetric, positive-definite matrix. After simple derivation, from Eq. (B16) we get

$$\begin{aligned}&\mathfrak{p}(\boldsymbol{\rho}_a, h_a, \phi_a, \boldsymbol{\rho}_b, h_b, \phi_b; \kappa, \mu, \tau) \\ &\quad = (4\pi^2\sqrt{\det \mathbb{M}})^{-1} \exp\left(-\tfrac{1}{2}\boldsymbol{\Phi}^{\mathrm{T}}\mathbb{M}^{-1}\boldsymbol{\Phi}\right),\end{aligned} \tag{B20}$$

where the prefactor is calculated from the normalization condition

$$\begin{aligned}&\int_{-\infty}^{\infty} dh_a \int_{-\infty}^{\infty} d\phi_a \int_{-\infty}^{\infty} dh_b \int_{-\infty}^{\infty} d\phi_b \\ &\quad \times \mathfrak{p}(\kappa, \mu, \tau; \boldsymbol{\rho}_a, h_a, \phi_a, \boldsymbol{\rho}_b, h_b, \phi_b) = 1\end{aligned} \tag{B21}$$

using Eq. (B19). Finally, we calculate the correlation functions using the relations

$$\int d\boldsymbol{v}\, v_i \exp\left(-\frac{1}{2}\boldsymbol{v}^{\mathrm{T}}\mathbb{A}\boldsymbol{v}\right) = 0, \tag{B22a}$$

$$\int d\boldsymbol{v}\, v_i v_j \exp\left(-\frac{1}{2}\boldsymbol{v}^{\mathrm{T}}\mathbb{A}\boldsymbol{v}\right) = \frac{(2\pi)^{n/2}}{\sqrt{\det \mathbb{A}}}(\mathbb{A}^{-1})_{ij}, \tag{B22b}$$

where v_i and v_j denote components of the n-dimensional vector $\boldsymbol{v}$; $\mathbb{A}$ is a symmetric, $n \times n$, positive-definite matrix; and $(\mathbb{A}^{-1})_{ij}$ denotes a component of the matrix $\mathbb{A}^{-1}$, i.e., the inverse of $\mathbb{A}$. After straightforward calculation we get

$$\mathfrak{C}_{hh}(\rho_{ab}) = \lim_{\Lambda\to\infty}(\langle h_a h_b\rangle - \langle h_a\rangle\langle h_b\rangle) = \lim_{\Lambda\to\infty}\bar{\mathfrak{C}}_{hh}(\rho_{ab}), \tag{B23a}$$

$$\mathfrak{C}_{h\phi}(\rho_{ab}) = \lim_{\Lambda\to\infty}(\langle h_a \phi_b\rangle - \langle h_a\rangle\langle \phi_b\rangle) = \lim_{\Lambda\to\infty}\bar{\mathfrak{C}}_{h\phi}(\rho_{ab}), \tag{B23b}$$

$$\mathfrak{C}_{\phi\phi}(\rho_{ab}) = \lim_{\Lambda\to\infty}(\langle \phi_a \phi_b\rangle - \langle \phi_a\rangle\langle \phi_b\rangle) = \lim_{\Lambda\to\infty}\bar{\mathfrak{C}}_{\phi\phi}(\rho_{ab}). \tag{B23c}$$

The result, together with Eq. (B15), proves the formulas in Eq. (10).

2. Order parameter profiles

We now move to the problem of finding the order parameter profiles in the system with N pinning points. The part of the Hamiltonian responsible for the pinning is $\mathcal{H}_{\mathrm{P}}$; see Eq. (6e). In order to include this term in our calculation of the path integrals we use the Hubbard-Stratonovich

transformation

$$\exp\left(-\beta\mathcal{H}_{\rm P}\right) = \prod_{i=1}^{N} \exp\left[-\frac{\nu}{2}[h(\rho_i)-h_i]^2\right] = \prod_{i=1}^{N} \frac{1}{\sqrt{2\pi\,\nu}} \int_{-\infty}^{\infty} d\psi_i \times \exp\left[-\frac{\psi_i^2}{2\nu} + i\psi_i[h(\rho_i)-h_i]\right], \quad \text{(B24)}$$

which in the limit $\nu \to \infty$ produces the same factor in the exponent as the Dirac delta function; see Eq. (B2). Therefore, neglecting the prefactor, the calculation of the path integrals goes along the same line as in the previous section and gives a formula similar to (B17).

In order to make the calculation as general as possible, we denote by x the order parameter for which we want to calculate the average ($x = h$ for height order parameter and $x = \phi$ for the composition order parameter) and denote its value in the point of interest $\boldsymbol{\rho}$ by x_0, i.e., $x(\boldsymbol{\rho}) = x_0$. If the membrane, following the pinning Hamiltonian $\mathcal{H}_{\rm P}$, is pinned in N additional points $\boldsymbol{\rho}_1, \boldsymbol{\rho}_2, \ldots \boldsymbol{\rho}_N$, where its height is fixed to $h_1, h_2, \ldots, h_N$, respectively, then, following the discussion presented in Sec. B 1, the probability is given by

$$\mathfrak{p}_x\left(\boldsymbol{\rho}, x_0, \{\boldsymbol{\rho}_i, h_i\}_{i=1}^N; \kappa, \mu, \tau\right) = \text{const} \prod_{i=0}^{N} \left(\int_{-\infty}^{\infty} d\psi_i\right) \exp\left[-\frac{1}{2}\bar{\mathfrak{C}}_{xx}(0)\psi_0^2 - \sum_{i=1}^{N} \bar{\mathfrak{C}}_{hx}(|\boldsymbol{\rho}_i - \boldsymbol{\rho}|)\psi_0\psi_i - \frac{1}{2}\sum_{i,j=1}^{N} \mathbb{B}_{ij}\psi_i\psi_j - i\psi_0 x_0 - i\sum_{i=1}^{N}\psi_i h_i\right], \quad \text{(B25)}$$

where the matrix $\mathbb{B}_{ij} = \bar{\mathfrak{C}}_{hh}(|\boldsymbol{\rho}_i - \boldsymbol{\rho}_j|)$. We now use Eq. (B19) to calculate the integrals over $\psi_1, \psi_2, \ldots, \psi_N$ in the above formula, and then Eq. (B8) to integrate over ψ_0. After straightforward calculation we get

$$\mathfrak{p}_x\left(\boldsymbol{\rho}, x_0, \{\boldsymbol{\rho}_i, h_i\}_{i=1}^N; \kappa, \mu, \tau\right) = \text{const}\exp\left\{-\frac{1}{2}\left[x_0^2 - 2x_0\sum_{i,j=1}^{N} h_i\bar{\mathfrak{C}}_{hx}(|\boldsymbol{\rho}_j - \boldsymbol{\rho}|)(\mathbb{B}^{-1})_{ij}\right] \times \left[\bar{\mathfrak{C}}_{xx}(0) - \sum_{i,j=1}^{N} \bar{\mathfrak{C}}_{hx}(|\boldsymbol{\rho}_i - \boldsymbol{\rho}|)\bar{\mathfrak{C}}_{hx}(|\boldsymbol{\rho}_j - \boldsymbol{\rho}|)(\mathbb{B}^{-1})_{ij}\right]^{-1}\right\}. \quad \text{(B26)}$$

After finding the constant from the normalization condition, we derive

$$\langle x(\boldsymbol{\rho})\rangle = \lim_{\Lambda\to\infty}\langle x_0\rangle = \lim_{\Lambda\to\infty}\int_{-\infty}^{\infty} dx_0\, x_0\, \mathfrak{p}_x\left(\boldsymbol{\rho}, x_0, \{\boldsymbol{\rho}_i, h_i\}_{i=1}^N; \kappa, \mu, \tau\right) = \lim_{\Lambda\to\infty}\sum_{i,j=1}^{N} h_i\bar{\mathfrak{C}}_{hx}(\boldsymbol{\rho}_j - \boldsymbol{\rho})(\mathbb{B}^{-1})_{ij}. \quad \text{(B27)}$$

We note that in the final formula for the order parameter profile, the limit $\Lambda \to \infty$ exists, as the correlation functions present in Eq. (B27) are all well defined in this limit.

In the case of $N = 1$ and $\rho_1 = \mathbf{0}$, we have $\mathbb{B} = [\bar{\mathfrak{C}}_{hh}(0)]$, and the formulas in Eq. (22) are recovered. In a different case of $h_1 = h_2 = \cdots = h_N \equiv h_0$ the formulas for the profile from [31] are verified.

APPENDIX C: BEHAVIOR OF THE ROOTS OF THE POLYNOMIAL W

In this Appendix we discuss the complex roots of the polynomial $W(z;\tau,\omega)$ given by Eq. (11). As we have pointed in the main text, the properties of the roots define three zones present in the model; see Fig. 2. In zone I the roots have the form $\pm it_1$, $\pm it_2$, and $\pm it_3$, with $t_1 < t_2 < t_3$. In zones II and III the six roots have the form $\pm it_1$ and $\pm a \pm it_2$, where $a, t_1, t_2 > 0$ and $t_1 < t_2$ in zone II and $t_1 > t_2$ in zone III.

We note, that all the above coefficients can in principle be calculated analytically with the help of Cardano's formula, as W is a third-order polynomial of z^2. Nevertheless, we keep the roots as parameters for the sake of simplicity.

The behavior of the parameters upon crossing the borders of the zones has been illustrated in Fig. 7. Upon going between zones II and III, the parameters $t_1(\omega,\tau)$, $t_2(\omega,\tau)$, and $a(\omega,\tau)$ are analytic functions. This is because the only difference between this zones is the relation between t_1 and t_2. On the contrary, going from zone I to zone II or III is accompanied with a rapid change of t_1 or t_2 as these functions have been differently defined in zone I. Upon approaching the border of zone I from zone II [Fig. 7(b)] t_1 and t_2 stay finite and a approaches zero. Exactly at the border, a is zero and t_2 (from zone II) splits into the parameters t_2 and t_3 (from zone I). The parameter t_1 stays analytic upon crossing this border. Upon approaching the border between zone I and III from the side of zone I, the parameters t_1 and t_2 approach each other. Exactly at the border they become equal and become t_2 from zone III. The parameter a from zone III is zero at the border and grows upon entering inside zone III. The parameter t_3 in zone I is analytic and is renamed t_1 in zone III. The behavior of the roots upon crossing the borders of zone I is similar to what happens to the roots of the polynomial $z^2 + c$ when c is continuously changed from positive to negative values.

In the special point $\omega^* = 8/(3\sqrt{3}) \approx 1.54$ and $\tau^* = 1/(6\sqrt{3}) \approx 0.0962$, where all three zones meet, the polynomial W has a pair of triple-degenerate roots equal to $\pm 3^{-1/4}\, i \approx \pm 1.32\, i$. This means that upon approaching to this point from zone I, the parameters t_1, t_2, and t_3 become equal; and upon approaching from zone II or III, parameters t_1 and t_2 become equal and a decays to zero.

APPENDIX D: CALCULATION OF INTEGRALS

In this Appendix we present the details of calculation of the integrals present in the formulas for the correlation functions in different zones. The calculation is based on a (simplified) method presented in [67]. Here we focus on Eq. (10b),

$$I = \int_0^{\infty} \frac{x\,\mathcal{J}_0(\rho\,x)}{(x^4+1)(x^2+2\tau+\omega)-\omega}\,dx, \quad \text{(D1)}$$

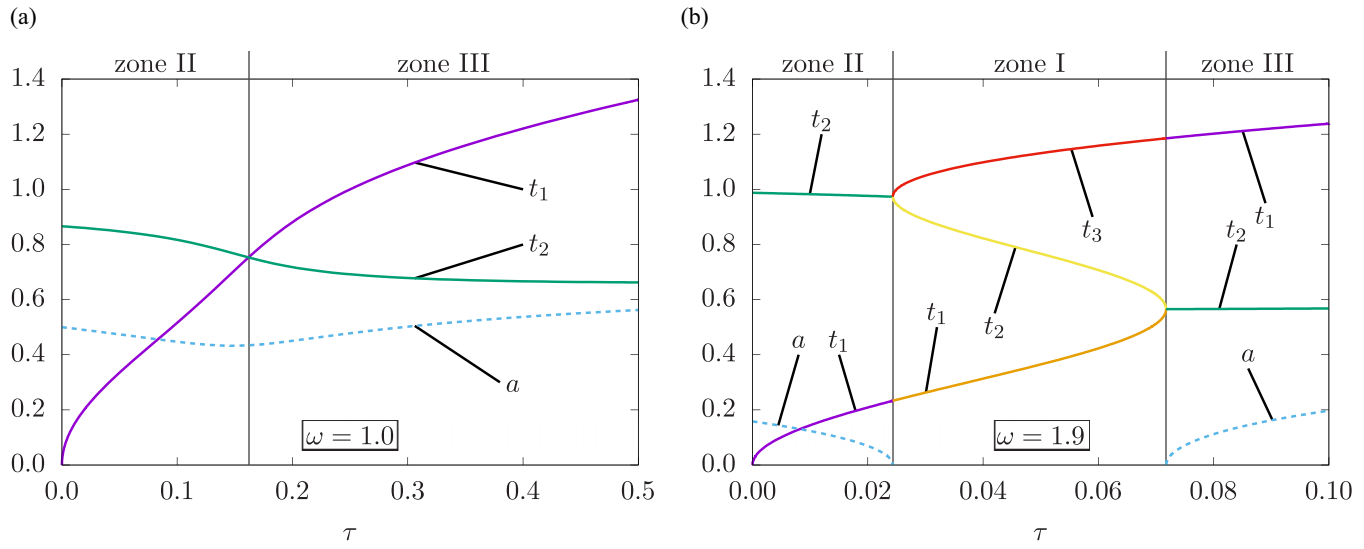

FIG. 7. Parameters t_1, t_2, t_3, and a that describe the complex roots of the polynomial $W(z;\omega,\tau)$ as a function of τ for fixed (a) $\omega = 1.0$, and (b) $\omega = 1.9$. The zones on the plane of parameters have been marked on top of the graphs, and gray vertical lines denote the borders between zones (see Fig. 2).

and assume that the parameters are in zone II or III, where the roots of the polynomial $W(z)$ are of the form $\pm i\,t_1$ and $\pm a \pm i\,t_2$; see Eq. (11). All other integrals can be calculated exactly the same way.

First, we note that the Bessel functions present in the calculation are analytical functions on the complex plane with a branch cut for a real, nonpositive argument. Moreover, if x is shifted infinitesimally towards positive imaginary values, the integrand becomes a symmetric function of its argument, and, therefore, we can extend the range of integration

$$I = \frac{1}{2}\lim_{\epsilon\to 0^+}\int_{-\infty+i\epsilon}^{\infty+i\epsilon}\frac{x\,\mathcal{J}_0(\rho\,x)}{(x^4+1)(x^2+2\tau+\omega)-\omega}\,dx. \quad \text{(D2)}$$

In the second step, the Bessel function $\mathcal{J}_0$ is replaced with the Hankel function of the first kind $\mathcal{H}_0^{(1)}(z) = \mathcal{J}_0(z) + i\,\mathcal{Y}_0(z)$, where $\mathcal{Y}_0$ denotes the (unmodified) Bessel function of the second kind. The resulting integral is

$$I = \frac{1}{2}\,\mathrm{Re}\left[\lim_{\epsilon\to 0^+}\int_{-\infty+i\epsilon}^{\infty+i\epsilon}\frac{x\,\mathcal{H}_0^{(1)}(\rho\,x)}{(x^4+1)(x^2+2\tau+\omega)-\omega}\,dx\right]. \quad \text{(D3)}$$

The advantage of this change is that $\mathcal{H}_0^{(1)}(z)$ for large $|z|$ behaves like $\exp(iz)$, and, therefore, we can close the contour of integration in (D3) with a large semicircle on the upper half of the complex plane. Now, the integral can be calculated using the residue theorem. For $\epsilon \to 0^+$ there are three poles of the integrand inside the contour of integration: the roots of the polynomial $W(z)$

$$z_1 = i\,t_1, \quad z_2 = a + i\,t_2, \quad \text{and} \quad z_3 = -a + i\,t_3. \quad \text{(D4)}$$

We thus get

$$I = \tfrac{1}{2}\,\mathrm{Re}\left\{2\pi i\left[\operatorname*{Res}_{z_1} f(z) + \operatorname*{Res}_{z_2} f(z) + \operatorname*{Res}_{z_3} f(z)\right]\right\}, \quad \text{(D5)}$$

where $f(z)$ denotes the integrand in (D3).

The last step is the calculation and simplification of (D5); this is done using the identity

$$\mathcal{H}_0^{(1)}(z) = -\frac{2i}{\pi}\mathcal{K}_0(-i\,z), \quad \text{(D6)}$$

valid for $\mathrm{Re}\,z > 0$ or $\mathrm{Im}\,z > 0$. After a short derivation we discover that the last two terms in Eq. (D5) are equal, and we recover Eq. (15b).

APPENDIX E: LIMITING CASES FOR THE CORRELATION FUNCTIONS

This Appendix is devoted to study of the properties of the correlation functions, defined in Sec. III, in various limiting cases. We concentrate here on the cases where the result can be related to other, already known models.

1. Limit $\tau \to \infty$ with κ and μ fixed

The limit $\tau \to \infty$ implies that the length scales fulfill the relation $\ell_\phi \ll \ell_h, \ell_{\text{coupling}}$. The parameter τ appears in the Hamiltonian of the model (6) in the term $\mathcal{H}_\text{G}$, where it is multiplied by $\phi^2(\boldsymbol{\rho})$. Therefore, the limit $\tau \to \infty$, with other parameters fixed, implies that $\phi(\boldsymbol{\rho}) \to 0$, which reduces the interaction to the membrane deformation Hamiltonian for the field $h(\boldsymbol{\rho})$. This observation is in line with the limiting value of the correlation length given by Eq. (18): in the membrane deformation model the correlation length (in units of ζ) is equal to $\sqrt{2}$.

In order to calculate the correlation functions in this limit we first note that for large values of τ the system is in zone III, and therefore, the formulas given in Eq. (15) must be used. In the second step we calculate the roots of the polynomial (11) in this limit and parameters associated with them. After some algebra we get for $\tau \to \infty$

$$t_1 = \sqrt{2\tau} + O(\tau^{-1/2}), \quad t_2 = a = \frac{1}{\sqrt{2}} + O(\tau^{-1}). \quad \text{(E1)}$$

Finally, we use the above result in Eq. (15). The first term in each of the formulas decays to zero for large τ like $\exp(-\sqrt{2\tau}\rho)$, and, for $\rho \neq 0$, it can be neglected in comparison with the second term. After simple calculation we derive

$$\mathfrak{C}_{hh}(\rho;\kappa,\tau\to\infty,\mu) = -\frac{1}{2\pi\kappa}\,\mathrm{kei}(\rho) + O(\tau^{-1}), \tag{E2a}$$

$$\mathfrak{C}_{h\phi}(\rho;\kappa,\tau\to\infty,\mu) = -\frac{\mu}{4\pi\tau}\,\mathrm{kei}\,(\rho) + O(\tau^{-2}), \tag{E2b}$$

$$\mathfrak{C}_{\phi\phi}(\rho;\kappa,\tau\to\infty,\mu) = -\frac{\kappa\mu^2}{8\pi\tau^2}\,\mathrm{kei}\,(\rho) + O(\tau^{-3}), \tag{E2c}$$

where $\mathrm{kei}(\rho) = \mathrm{Im}\,\mathcal{K}_0[\rho(1+i)/\sqrt{2}]$ denotes the Kelvin function kei.

The result for the correlation function $\mathfrak{C}_{hh}$ [Eq. (E2a)] is in full agreement with the result known for the membrane deformation model [49,66]. The disappearing of the correlation functions $\mathfrak{C}_{h\phi}$ and $\mathfrak{C}_{\phi\phi}$ in the limit $\tau\to\infty$ is caused by the vanishing of the order parameter ϕ in this limit.

We note that the limiting correlation function $\mathfrak{C}_{\phi\phi}$ [given by Eq. (E2c)] is finite for $\rho = 0$, even though for any finite τ the function diverges logarithmically [see Eq. (14)]. The disagreement shows that in this case the limit $\tau\to\infty$ is not uniform—for any finite τ there is a region around $\rho = 0$, where the value of $\mathfrak{C}_{\phi\phi}(\rho;\kappa,\tau,\mu)$ is essentially different from $\mathfrak{C}_{\phi\phi}(\rho;\kappa,\tau\to\infty,\mu)$, but the size of this region shrinks $\sim\tau^{-1/2}$ upon increasing τ.

2. Limit $\tau \to 0$ with κ and μ fixed

We now move to the opposite limit $\tau\to 0$, i.e., to the case $\ell_h, \ell_{\mathrm{coupling}} \ll \ell_\phi$. In this regime the Gaussian model is known to be critical [68]. Since, as discussed in Sec. III E, in our model the correlation length diverges for small values of τ, here we also expect criticality.

We start the analysis by noting that for $\tau\to 0$ the system can be either in zone I or in zone II. For $\omega \geqslant 2$, the system is in zone I, the parameters describing the roots of polynomial (11) are

$$t_1 = \sqrt{2\tau} + O(\tau^{3/2}), \tag{E3a}$$

$$t_2 = (\omega - \sqrt{\omega^2-4})^{1/2}/\sqrt{2} + O(\tau), \tag{E3b}$$

$$t_3 = (\omega + \sqrt{\omega^2-4})^{1/2}/\sqrt{2} + O(\tau), \tag{E3c}$$

and the correlation functions are given by Eq. (12). For $\omega < 2$, the system is in zone II, the parameters are

$$t_1 = \sqrt{2\tau} + O(\tau^{3/2}), \tag{E4a}$$

$$t_2 = \sqrt{2+\omega}/2 + O(\tau), \tag{E4b}$$

$$a = \sqrt{2-\omega}/2 + O(\tau), \tag{E4c}$$

and the correlation functions are given by Eq. (15). The special case of $\omega = 2$ has been incorporated into the first case above, because for small nonzero τ and $\omega = 2$, the system is in zone I, just like for $\omega > 2$.

For fixed ρ and $\tau\to 0$ we derive the following formulas for the correlation functions (the calculations were done separately for the system in zone I and in zone II giving the same results):

$$\mathfrak{C}_{hh}(\rho;\kappa,\tau\to 0,\mu) = -\frac{\mu^2\ln\tau}{4\pi} + O(1), \tag{E5a}$$

$$\mathfrak{C}_{h\phi}(\rho;\kappa,\tau\to 0,\mu) = -\frac{\mu\ln\tau}{4\pi} + O(1), \tag{E5b}$$

$$\mathfrak{C}_{\phi\phi}(\rho;\kappa,\tau\to 0,\mu) = -\frac{\ln\tau}{4\pi} + O(1). \tag{E5c}$$

All the functions do not depend on ρ, which means that the fluctuations keep both order parameters constant. This is not surprising since for $\tau\to 0$ the correlation length ξ diverges, and thus keeping ρ fixed implies the regime $\rho \ll \xi$ in which the correlation function is expected to stay almost constant. Moreover, the relation $\mathfrak{C}_{hh} = \mu\mathfrak{C}_{h\phi} = \mu^2\mathfrak{C}_{\phi\phi}$ implies that the coupling between order parameters given by Eq. (6d) is strictly fulfilled (at least in the leading order). We note that all the correlation functions diverge logarithmically for $\tau\to 0$.

To gain more insight into the behavior of the correlation functions for small τ, it is useful to introduce the scaling limit $\tau\to 0$, $\rho\to\infty$ with the scaling variable $u = \sqrt{2\tau}\rho \approx \rho/\xi$ fixed. In this limit, after some algebra, we get

$$\mathfrak{C}_{hh}(u;\kappa,\tau\to 0,\mu) = \frac{\mu^2\mathcal{K}_0(u)}{2\pi} + O(\tau), \tag{E6a}$$

$$\mathfrak{C}_{h\phi}(u;\kappa,\tau\to 0,\mu) = \frac{\mu\mathcal{K}_0(u)}{2\pi} + O(\tau), \tag{E6b}$$

$$\mathfrak{C}_{\phi\phi}(u;\kappa,\tau\to 0,\mu) = \frac{\mathcal{K}_0(u)}{2\pi} + O(\tau). \tag{E6c}$$

This result should be compared with the prediction for systems in the vicinity of a critical point based on the scaling hypothesis [71]

$$\mathfrak{C} = \rho^{-(d-2+\eta)}\mathcal{C}(u), \tag{E7}$$

where $d = 2$ is the dimensionality of the system, η is a critical exponent, and $\mathcal{C}(u)$ is a universal scaling function. We note that only $\mathfrak{C}_{\phi\phi}$ is strictly following Eq. (E7), with $\eta = 0$ (the same value as in Gaussian model) and $\mathcal{C}(u) = \mathcal{K}_0(u)/(2\pi)$ (see, e.g., [68]); the scaling formulas for $\mathfrak{C}_{hh}$ and $\mathfrak{C}_{h\phi}$ contain an additional nonuniversal (depending on the coupling μ) factor. Like in the case of fixed ρ, the correlation functions in the leading order differ only by the power of μ, which implies that the order parameters are strongly coupled. This explains why both order parameters become critical in the limit $\tau\to 0$ and the divergence of all the correlation functions (E6) for $u\to 0$.

3. Limit $\mu \to 0$ with κ and τ fixed

We now consider the case of $\mu\to 0$, i.e., when the two order parameters are weakly coupled. This implies that $\ell_h, \ell_\phi \ll \ell_{\mathrm{coupling}}$. In this limit, depending on the value of τ, the system is in zone II or III, and therefore, the correlation functions are given by Eq. (15).

We start from expanding the roots of the polynomial (11) in the limit of small $\omega = \kappa\mu^2$. After some algebra we get

$$t_1 = \sqrt{2\tau} + \frac{\sqrt{2}\tau^{3/2}\omega}{1+4\tau^2} + O(\omega^2), \tag{E8a}$$

$$t_2 = \frac{1}{\sqrt{2}} + \frac{(1-2\tau)\omega}{4\sqrt{2}(1+4\tau^2)} + O(\omega^2), \tag{E8b}$$

$$a = \frac{1}{\sqrt{2}} - \frac{(1+2\tau)\omega}{4\sqrt{2}(1+4\tau^2)} + O(\omega^2), \tag{E8c}$$

and the same expansion is valid for both zones II and III. This allows us to calculate the correlation length in this limit

$$\xi(\tau, \omega \to 0) = \max((2\tau)^{-1/2}, \sqrt{2}) + O(\omega), \tag{E9}$$

which is in agreement with the plots of the correlation length in Fig. 4(a).

Using Eq. (E8) in Eq. (15) we derive the asymptotic form of the correlation functions:

$$\mathfrak{C}_{hh}(\rho;\kappa,\tau,\mu\to 0) = \frac{\mu^2 \mathcal{K}_0(\rho\sqrt{2\tau})}{2\pi(1+4\tau^2)^2} - \frac{\mathrm{kei}\,(\rho)}{2\pi\kappa}, \tag{E10a}$$

$$\mathfrak{C}_{h\phi}(\rho;\kappa,\tau,\mu\to 0) = \frac{\mu\,\mathcal{K}_0(\rho\sqrt{2\tau})}{2\pi(1+4\tau^2)} - \frac{\mu[2\tau\,\mathrm{kei}\,(\rho) + \mathrm{ker}\,(\rho)]}{2\pi(1+4\tau^2)}, \tag{E10b}$$

$$\mathfrak{C}_{\phi\phi}(\rho;\kappa,\tau,\mu\to 0) = \frac{\mathcal{K}_0(\rho\sqrt{2\tau})}{2\pi} + \frac{\kappa\mu^2[(1-4\tau^2)\,\mathrm{kei}(\rho) - 4\tau\,\mathrm{ker}(\rho)]}{2\pi(1+4\tau^2)^2}, \tag{E10c}$$

where we have introduced another Kelvin function $\mathrm{ker}(\rho) = \mathrm{Re}\,\mathcal{K}_0[\rho(1+i)/\sqrt{2}]$. In Eqs. (E10) we have calculated the leading term separately for the two terms present in the formula for each of the correlation functions in Eq. (15); the neglected, higher order terms were always smaller at least by a factor of μ^2.

Each of the formulas for the correlation functions (E10) consists of two terms: the first term, proportional to $\mathcal{K}_0(\rho\sqrt{2\tau})$, for large ρ decays exponentially to zero with a length scale $(2\tau)^{-1/2}$; the second term, proportional to the combination of $\mathrm{kei}(\rho)$ and $\mathrm{ker}(\rho)$, for large ρ decays exponentially to zero with a length scale $\sqrt{2}$. For $\tau < 1/4$ (i.e., in zone II) the former length scale is bigger, and, therefore, for $\mu \neq 0$ all correlation functions decay with the same length scale $(2\tau)^{-1/2}$, in line with Eq. (E9). Nevertheless, upon decreasing μ to 0, the amplitudes multiplying the first term in Eq. (E10a), both terms in Eq. (E10b), and the second term in Eq. (E10c) are decaying to 0. As a result for $\mu = 0$ the function $\mathfrak{C}_{hh}$ decays to zero with a length scale $\sqrt{2}$, $\mathfrak{C}_{h\phi}$ is zero, and $\mathfrak{C}_{\phi\phi}$ decays to zero with the original length scale $(2\tau)^{-1/2}$. For $\tau \geqslant 1/4$ (i.e., in zone III) for $\mu > 0$ the second terms in formulas (E10) dominate, and all correlation functions decay with a length scale $\sqrt{2}$. For $\mu = 0$, due to zeroing of some amplitudes, the same result as for $\tau < 1/4$ is recovered.

The above analysis shows that, even though the correlation functions change for $\mu \to 0$ in a continuous manner, the correlation length is discontinuous at $\mu = 0$: For $\mu > 0$ the correlation length is the same for all correlation functions, and it is given by Eq. (E9). For $\mu = 0$, we have

$$\mathfrak{C}_{hh}(\rho;\kappa,\tau,\mu=0) = -\frac{\mathrm{kei}\,(\rho)}{2\pi\kappa}, \tag{E11a}$$

$$\mathfrak{C}_{h\phi}(\rho;\kappa,\tau,\mu=0) = 0, \tag{E11b}$$

$$\mathfrak{C}_{\phi\phi}(\rho;\kappa,\tau,\mu=0) = \frac{\mathcal{K}_0(\rho\sqrt{2\tau})}{2\pi}, \tag{E11c}$$

i.e., the correlation function $\mathfrak{C}_{hh}$ decays to zero with a length scale $\sqrt{2}$ and the correlation function $\mathfrak{C}_{\phi\phi}$ with a length scale $(2\tau)^{-1/2}$, and there is no correlation between the order parameters. We note that Eq. (E11a) agrees with the correlation function in the membrane deformation model and Eq. (E11c) with the correlation function in Gaussian model [see Eq. (E2a) and Refs. [66,68]].

4. Limit $\mu \to \infty$ with κ and τ fixed

The effect of this limiting case, in which $\ell_{\mathrm{coupling}} \ll \ell_h, \ell_\phi$, is not evident at first sight. In order to study and explain the behavior of the system, we first note that in the limit $\mu \to \infty$ the system is for $\tau > 0$ in zone III; see Fig. 2. In this zone the roots of the polynomial (11) are described by three parameters t_1, t_2, and a. For large μ we have calculated

$$t_1 = \mu\sqrt{\kappa} + \frac{\tau}{\mu\sqrt{\kappa}} + O(\mu^{-3}), \tag{E12a}$$

$$t_2 = \left(\frac{\tau}{2\kappa}\right)^{1/4} \mu^{-1/2} + O(\mu^{-3/2}), \tag{E12b}$$

$$a = (2\tau/\omega)^{1/4}/\sqrt{2} + O(\omega^{-3/4}), \tag{E12c}$$

which implies

$$\xi = 1/t_2 = \left(\frac{2\kappa}{\tau}\right)^{1/4} \sqrt{\mu} + O(\mu^{-1/2}) \to \infty, \tag{E13}$$

and, therefore, in the limit $\mu \to \infty$ the system becomes critical. By substituting Eq. (E12) into Eq. (15), for fixed ρ (i.e., for $\rho \ll \xi$ when $\mu \to \infty$) we get

$$\mathfrak{C}_{hh}(\rho;\kappa,\tau,\mu\to\infty) = \frac{\mu}{8\sqrt{2\tau\kappa}} + O(\ln\mu), \tag{E14a}$$

$$\mathfrak{C}_{h\phi}(\rho;\kappa,\tau,\mu\to\infty) = \frac{1}{8\sqrt{2\tau\kappa}} + O\left(\frac{\ln\mu}{\mu}\right), \tag{E14b}$$

$$\mathfrak{C}_{\phi\phi}(\rho;\kappa,\tau,\mu\to\infty) = \frac{1}{8\mu\sqrt{2\tau\kappa}} + O\left(\frac{\ln\mu}{\mu^2}\right), \tag{E14c}$$

which shows that in this limit both order parameters stay constant on the length scale ξ (the same behavior we have seen in the limit $\tau \to 0$; see Sec. E 2). The value of field $h(\boldsymbol{\rho})$ fluctuates with a standard deviation that scales like $\sqrt{\mu}$, and the field $\phi(\boldsymbol{\rho})$ has a standard deviation $\sim 1/\sqrt{\mu}$. Therefore, for large μ the Gaussian term (6c) in the Hamiltonian (6a) becomes negligible. This, in turn, allows the field ϕ to adapt to changes of the field h at no additional energy cost (which is in line with the fact that in this limit $\ell_{\mathrm{coupling}} \to 0$) and makes the coupling term (6d) also negligible. Without pinning, the only relevant term left in the Hamiltonian is (6b) which allows for large-scale fluctuations of the membrane [72]. The behavior of our system in the limit $\mu \to \infty$ can thus be identified with the critical roughening of the membrane.

Finally, to describe the correlation functions in the limit $\mu \to \infty$ it is useful to introduce the scaling variable $v = \rho/\xi = \rho\, t_2 \sim \rho/\sqrt{\mu}$. As we have checked, in the scaling limit $\mu \to \infty$ with v fixed we get

$$\mathfrak{C}_{hh}(v;\kappa,\tau,\mu\to\infty) = \frac{\mathrm{kei}(\sqrt{2}v)\mu}{\pi\sqrt{8\tau\kappa}} + O(\mu^{-3}), \quad \text{(E15a)}$$

$$\mathfrak{C}_{h\phi}(v;\kappa,\tau,\mu\to\infty) = \frac{\mathrm{kei}(\sqrt{2}v)}{\pi\sqrt{8\tau\kappa}} + O(\mu^{-2}), \quad \text{(E15b)}$$

$$\mathfrak{C}_{\phi\phi}(v;\kappa,\tau,\mu\to\infty) = \frac{\mathrm{kei}(\sqrt{2}v)}{\pi\sqrt{8\tau\kappa\mu}} + O(\mu^{-3}). \quad \text{(E15c)}$$

5. Limit of strong binding between order parameters

Another interesting limiting case is when the binding γ between two order parameters is going to ∞. In this limit $\ell_{\mathrm{coupling}} \ll \ell_h \ll \ell_\phi$. From Eq. (3) it follows that the two order parameters must strictly fulfill the relation $\bar{h}(\mathbf{r}) = \alpha\bar{\phi}(\mathbf{r})$, and the system is effectively described by a single order parameter. In this case the Hamiltonian reduces to

$$\beta\tilde{\mathcal{H}} = \int d\mathbf{r}\left\{\frac{\kappa}{2}[\nabla^2\bar{h}(\mathbf{r})]^2 + \frac{\tilde{\sigma}}{2}[\nabla\bar{h}(\mathbf{r})]^2 + \frac{\tilde{\gamma}}{2}\bar{h}^2(\mathbf{r}) + \frac{\lambda}{2}\sum_{i=1}^{N}[\bar{h}(\mathbf{r}_i) - \ell_i]^2\right\}, \quad \text{(E16)}$$

with $\tilde{\sigma} = \sigma/\alpha^2$ and $\tilde{\gamma} = 2t/\alpha^2$. The above Hamiltonian has already been discussed in the literature [53], as it describes a membrane with binding stiffness κ and surface tension $\tilde{\sigma}$ in an external harmonic potential of the strength $\tilde{\gamma}$. The results of our model, after taking the proper limit (as described below), are in full agreement with [53].

The limit $\gamma \to \infty$ implies that $\zeta = (\kappa/\gamma)^{1/4} \to 0$, and thus, $\tau \to 0$ and $\mu \to \infty$ (see Table I) with fixed

$$\kappa\tau\mu^2 = \tau\omega = \frac{t\kappa\alpha^2}{\sigma^2} \equiv \frac{1}{8}\chi^2, \quad \text{(E17)}$$

where, in order to simplify the notation, we have added an extra factor κ, and we have defined $\chi \geqslant 0$. The vanishing of the unit of length ζ makes the analysis of this special limit challenging.

In Fig. 2 the limit considered here is located in the region where the border between zones I and III asymptotically touches the line $\tau = 0$. Closer analysis shows that in this limit the system is in zone I for $\chi < 1$ (and the correlation function decays exponentially) and in zone III for $\chi > 1$ (where $\mathfrak{C}_{hh}$ shows damped oscillations). The same change of asymptotics has been reported in [53] for $\sigma/\lambda_{\mathrm{m}}^0 = 1/4$, which is in an agreement with our results since $\sigma/\lambda_{\mathrm{m}}^0$ in [53] is equivalent to $(4\chi)^{-1}$ in our paper.

Detailed analysis of the roots of the polynomial (11) shows that in this limit for $\chi < 1$ (zone I)

$$t_1 = \frac{2}{\chi}\sqrt{1-\sqrt{1-\chi^2}}\,\tau^{1/2} + O(\tau^{3/2}), \quad \text{(E18a)}$$

$$t_2 = \frac{2}{\chi}\sqrt{1+\sqrt{1-\chi^2}}\,\tau^{1/2} + O(\tau^{3/2}), \quad \text{(E18b)}$$

$$t_3 = \frac{\chi}{2\sqrt{2\tau}} + O(\tau^{1/2}), \quad \text{(E18c)}$$

and for $\chi > 1$ (zone III)

$$a = \frac{\sqrt{2\tau}}{\chi}\sqrt{\chi-1} + O(\tau^{3/2}), \quad \text{(E19a)}$$

$$t_1 = \frac{\chi}{2\sqrt{2\tau}} + O(\tau^{1/2}), \quad \text{(E19b)}$$

$$t_2 = \frac{\sqrt{2\tau}}{\chi}\sqrt{\chi+1} + O(\tau^{3/2}). \quad \text{(E19c)}$$

Therefore, the (dimensional) correlation length $\bar{\xi}$ is for $\chi < 1$ (zone I)

$$\bar{\xi} = \zeta\xi = \frac{\zeta}{t_1} = \left(\frac{\chi}{1-\sqrt{1-\chi^2}}\right)^{1/2}\tilde{\zeta}, \quad \text{(E20)}$$

and for $\chi > 1$ (zone III)

$$\bar{\xi} = \zeta\xi = \frac{\zeta}{t_2} = \left[\frac{2\chi}{(\chi+1)}\right]^{1/2}\tilde{\zeta}, \quad \text{(E21)}$$

with $\tilde{\zeta} = (\kappa/\tilde{\gamma})^{1/4}$. The above formula for the correlation length can be shown to be identical with Eq. (36) in [53]. We note that, even though in this limit two different critical regimes $\tau \to 0$ and $\mu \to \infty$ overlap, only the dimensionless correlation length ξ is infinite. Together with increasing ξ, the unit of length $\zeta \to 0$, which keeps the dimensional correlation length $\bar{\xi} = \zeta\xi$ finite, and the system is actually not critical.

Because our notation makes the analysis of this limit unnecessarily complicated, we refrain from a detailed study of our model for $\gamma \to 0$. Properties of the model in this special case have been discussed in [53].

[1] C. Dietrich, L. A. Bagatolli, Z. N. Volovyk, N. L. Thompson, M. Levi, K. Jacobson, and E. Gratton, Lipid rafts reconstituted in model membranes, Biophys. J. **80**, 1417 (2001).

[2] S. L. Veatch, O. Soubias, S. L. Keller, and K. Gawrisch, Critical fluctuations in domain-forming lipid mixtures, Proc. Natl. Acad. Sci. USA **104**, 17650 (2007).

[3] A. R. Honerkamp-Smith, S. L. Veatch, and S. L. Keller, An introduction to critical points for biophysicists; observations of compositional heterogeneity in lipid membranes, Biochim. Biophys. Acta Biomembr. **1788**, 53 (2009).

[4] M. B. Stone, S. A. Shelby, and S. L. Veatch, Super-resolution microscopy: Shedding light on the cellular plasma membrane, Chem. Rev. **117**, 7457 (2017).

[5] S. Voci, B. Goudeau, G. Valenti, A. Lesch, M. Jović, S. Rapino, F. Paolucci, S. Arbault, and N. Sojic, Surface-confined electrochemiluminescence microscopy of cell membranes, J. Am. Chem. Soc. **140**, 14753 (2018).

[6] C. Roobala, I. Ilanila, and J. Basu, Applications of sted fluorescence nanoscopy in unravelling nanoscale structure and dynamics of biological systems, J. Biosci. **43**, 471 (2018).

[7] P. E. Wright and H. J. Dyson, Intrinsically disordered proteins in cellular signalling and regulation, Nat. Rev. Mol. Cell Biol. **16**, 18 (2015).

[8] J. Hancock, *Cell Signalling* (Oxford University Press, Oxford, 2017).

[9] M. B. Stone, S. A. Shelby, M. F. Núñez, K. Wisser, and S. L. Veatch, Protein sorting by lipid phase-like domains supports emergent signaling function in B lymphocyte plasma membranes, eLife **6**, e19891 (2017).

[10] R. Dimova and C. Marques (eds.), *The Giant Vesicle Book* (CRC Press, Boca Raton, FL, 2019).

[11] Q. Xiao, C. K. McAtee, and X. Su, Phase separation in immune signalling, Nat. Rev. Immunol. **22**, 188 (2022).

[12] I. Levental and E. Lyman, Regulation of membrane protein structure and function by their lipid nano-environment, Nat. Rev. Mol. Cell Biol. **24**, 107 (2023).

[13] D. Meder, M. J. Moreno, P. Verkade, W. L. C. Vaz, and K. Simons, Phase coexistence and connectivity in the apical membrane of polarized epithelial cells, Proc. Natl. Acad. Sci. USA **103**, 329 (2006).

[14] A. Pralle, P. Keller, E.-L. Florin, K. Simons, and J. K. H. Hörber, Sphingolipid–cholesterol rafts diffuse as small entities in the plasma membrane of mammalian cells, J. Cell Biol. **148**, 997 (2000).

[15] I. Levental, K. R. Levental, and F. A. Heberle, Lipid rafts: Controversies resolved, mysteries remain, Trends Cell Biol. **30**, 341 (2020).

[16] P.-F. Lenne and A. Nicolas, Physics puzzles on membrane domains posed by cell biology, Soft Matter **5**, 2841 (2009).

[17] N. Destainville, M. Manghi, and J. Cornet, A rationale for mesoscopic domain formation in biomembranes, Biomolecules **8**, 104 (2018).

[18] T. Gil, M. C. Sabra, J. H. Ipsen, and O. G. Mouritsen, Wetting and capillary condensation as means of protein organization in membranes, Biophys. J. **73**, 1728 (1997).

[19] T. Gil, J. H. Ipsen, O. G. Mouritsen, M. C. Sabra, M. M. Sperotto, and M. J. Zuckermann, Theoretical analysis of protein organization in lipid membranes, Biochim. Biophys. Acta Rev. Biochim. **1376**, 245 (1998).

[20] J. C. Owicki, M. W. Springgate, and H. M. McConnell, Theoretical study of protein-lipid interactions in bilayer membranes, Proc. Natl. Acad. Sci. USA **75**, 1616 (1978).

[21] A. Hanke and S. Dietrich, Critical adsorption on curved objects, Phys. Rev. E **59**, 5081 (1999).

[22] A. R. Honerkamp-Smith, P. Cicuta, M. D. Collins, S. L. Veatch, M. Den Nijs, M. Schick, and S. L. Keller, Line tensions, correlation lengths, and critical exponents in lipid membranes near critical points, Biophys. J. **95**, 236 (2008).

[23] M. Venturoli, B. Smit, and M. M. Sperotto, Simulation studies of protein-induced bilayer deformations, and lipid-induced protein tilting, on a mesoscopic model for lipid bilayers with embedded proteins, Biophys. J. **88**, 1778 (2005).

[24] A.-F. Bitbol, D. Constantin, and J.-B. Fournier, Bilayer elasticity at the nanoscale: The need for new terms, PLoS ONE **7**, e48306 (2012).

[25] S. Leibler and D. Andelman, Ordered and curved mesostructures in membranes and amphiphilic films, J. Phys. France **48**, 2013 (1987).

[26] P. F. Devaux, Is lipid translocation involved during endo- and exocytosis?, Biochimie **82**, 497 (2000).

[27] P. Sens and S. A. Safran, Inclusions induced phase separation in mixed lipid film, Eur. Phys. J. E **1**, 237 (2000).

[28] J. Zimmerberg and M. M. Kozlov, How proteins produce cellular membrane curvature, Nat. Rev. Mol. Cell Biol. **7**, 9 (2006).

[29] D. Brown and E. London, Structure and origin of ordered lipid domains in biological membranes, J. Membr. Biol. **164**, 103 (1998).

[30] A. Shrestha, O. Kahraman, and C. A. Haselwandter, Regulation of membrane proteins through local heterogeneity in lipid bilayer thickness, Phys. Rev. E **102**, 060401(R) (2020).

[31] B. H. Stumpf, P. Nowakowski, C. Eggeling, A. Maciołek, and A.-S. Smith, Protein induced lipid demixing in homogeneous membranes, Phys. Rev. Res. **3**, L042013 (2021).

[32] E. Sackmann and R. Bruinsma, Cell adhesion as wetting transition?, in *Physics of Bio-molecules and Cells, Physique des biomolécules et des cellules*, edited by F. Flyvbjerg, F. Jülicher, P. Ormos, and F. David (Springer, Berlin, 2002), pp. 285–309.

[33] R. Bruinsma, A. Behrisch, and E. Sackmann, Adhesive switching of membranes: Experiment and theory, Phys. Rev. E **61**, 4253 (2000).

[34] E. Sackmann and A.-S. Smith, Physics of cell adhesion: Some lessons from cell-mimetic systems, Soft Matter **10**, 1644 (2014).

[35] S. F. Fenz, T. Bihr, D. Schmidt, R. Merkel, U. Seifert, K. Sengupta, and A.-S. Smith, Membrane fluctuations mediate lateral interaction between cadherin bonds, Nat. Phys. **13**, 906 (2017).

[36] B. H. Stumpf, A. Ambrović-Ristov, A. Radenovic, and A.-S. Smith, Recent advances and prospects in the research of nascent adhesions, Front. Physiol. **11**, 574371 (2020).

[37] M. L. Dustin, What counts in the immunological synapse?, Mol. Cell **54**, 255 (2014).

[38] E. Toledo, G. L. Saux, A. Edri, L. Li, M. Rosenberg, Y. Keidar, V. Bhingardive, O. Radinsky, U. Hadad, C. D. Primo *et al.*, Molecular-scale spatio-chemical control of the activating-inhibitory signal integration in NK cells, Sci. Adv. **7**, eabc1640 (2021).

[39] A. Honigmann, S. Sadeghi, J. Keller, S. W. Hell, C. Eggeling, and R. Vink, A lipid bound actin meshwork organizes liquid phase separation in model membranes, eLife **3**, e01671 (2014).

[40] S. A. Rautu, G. Rowlands, and M. S. Turner, Membrane Composition Variation and Underdamped Mechanics near Transmembrane Proteins and Coats, Phys. Rev. Lett. **114**, 098101 (2015).

[41] G. S. Ayton, J. L. McWhirter, P. McMurtry, and G. A. Voth, Coupling field theory with continuum mechanics: A simulation of domain formation in giant unilamellar vesicles, Biophys. J. **88**, 3855 (2005).

[42] A. Veksler and N. S. Gov, Phase transitions of the coupled membrane-cytoskeleton modify cellular shape, Biophys. J. **93**, 3798 (2007).

[43] S. Sadeghi, M. Müller, and R. L. C. Vink, Raft formation in lipid bilayers coupled to curvature, Biophys. J. **107**, 1591 (2014).

[44] M. Simunovic, E. Evergren, I. Golushko, C. Prévost, H.-F. Renard, L. Johannes, H. T. McMahon, V. Lorman, G. A. Voth, and P. Bassereau, How curvature-generating proteins build scaffolds on membrane nanotubes, Proc. Natl. Acad. Sci. USA **113**, 11226 (2016).

[45] C. Prévost, H. Zhao, J. Manzi, E. Lemichez, P. Lappalainen, A. Callan-Jones, and P. Bassereau, IRSp53 senses negative mem-

brane curvature and phase separates along membrane tubules, Nat. Commun. **6**, 8529 (2015).
[46] N. Dan, P. Pincus, and S. Safran, Membrane-induced interactions between inclusions, Langmuir **9**, 2768 (1993).
[47] N. Dan, A. Berman, P. Pincus, and S. A. Safran, Membrane-induced interactions between inclusions, J. Phys. II France **4**, 1713 (1994).
[48] J.-B. Fournier, Microscopic membrane elasticity and interactions among membrane inclusions: Interplay between the shape, dilation, tilt and tilt-difference modes, Eur. Phys. J. B **11**, 261 (1999).
[49] D. Nelson, T. Piran, and S. Weinberg, *Statistical Mechanics of Membranes and Surfaces* (World Scientific, Singapore, 2004).
[50] R. Lipowsky and E. Sackmann, *Structure and Dynamics of Membranes—From Cells to Vesicles*, Handbook of Biological Physics, Vol. 1 (Elsevier Science, Amsterdam, 1995).
[51] W. Helfrich, Elastic properties of lipid bilayers: Theory and possible experiments, Z. Naturforsch. C: Biosci. **28**, 693 (1973).
[52] R. Bruinsma, M. Goulian, and P. Pincus, Self-assembly of membrane junctions., Biophys. J. **67**, 746 (1994).
[53] J. A. Janeš, H. Stumpf, D. Schmidt, U. Seifert, and A.-S. Smith, Statistical mechanics of an elastically pinned membrane: Static profile and correlations, Biophys. J. **116**, 283 (2019).
[54] T. Ursell, K. C. Huang, E. Peterson, and R. Phillips, Cooperative gating and spatial organization of membrane proteins through elastic interactions, PLoS Comput. Biol. **3**, e81 (2007).
[55] C. A. Haselwandter and R. Phillips, Connection between oligomeric state and gating characteristics of mechanosensitive ion channels, PLoS Comput. Biol. **9**, e1003055 (2013).
[56] For example, using the experimental values and notation from [24], we get $\vartheta = K_a' d_0/\sqrt{K_a K_a''} \approx 0.89$.
[57] S. Leibler, Curvature instability in membranes, J. Phys. France **47**, 507 (1986).
[58] U. Seifert and R. Lipowsky, Adhesion of vesicles, Phys. Rev. A **42**, 4768 (1990).
[59] R. Lipowsky and S. Leibler, Unbinding Transitions of Interacting Membranes, Phys. Rev. Lett. **56**, 2541 (1986).
[60] G. Fragneto, T. Charitat, F. Graner, K. Mecke, L. Perino-Gallice, and E. Bellet-Amalric, A fluid floating bilayer, Europhys. Lett. **53**, 100 (2001).
[61] K. R. Mecke, T. Charitat, and F. Graner, Fluctuating lipid bilayer in an arbitrary potential: Theory and experimental determination of bending rigidity, Langmuir **19**, 2080 (2003).
[62] R. Blackwell, A. Hemmerle, A. Baer, M. Späth, W. Peukert, D. Parsons, K. Sengupta, and A.-S. Smith, On the control of dispersion interactions between biological membranes and protein coated biointerfaces, J. Colloid Interface Sci. **598**, 464 (2021).
[63] R. R. Netz, Inclusions in fluctuating membranes: Exact results, J. Phys. I France **7**, 833 (1997).
[64] P. Dommersnes and J.-B. Fournier, N-body study of anisotropic membrane inclusions: Membrane mediated interactions and ordered aggregation, Eur. Phys. J. B **12**, 9 (1999).
[65] The parameter ζ is often called the correlation length, but in the model with no composition order parameter the length scale at which the correlation function decays is $\sqrt{2}\zeta$.
[66] T. Bihr, U. Seifert, and A.-S. Smith, Multiscale approaches to protein-mediated interactions between membranes—Relating microscopic and macroscopic dynamics in radially growing adhesions, New J. Phys. **17**, 083016 (2015).
[67] Q.-G. Lin, Infinite integrals involving Bessel functions by contour integration, Integr. Transforms Special Funct. **24**, 783 (2013).
[68] N. Goldenfeld, *Lectures on Phase Transitions and the Renormalization Group*, Frontiers in Physics, Vol. 85 (CRC Press, Boca Raton, FL, 1992).
[69] M. E. Fisher and B. Wiodm, Decay of correlations in linear systems, J. Chem. Phys. **50**, 3756 (1969); Publisher's note: "Decay of correlations in linear systems", **143**, 209903 (2015).
[70] R. Evans, R. Leote de Carvalho, J. Henderson, and D. Hoyle, Asymptotic decay of correlations in liquids and their mixtures, J. Chem. Phys. **100**, 591 (1994).
[71] L. P. Kadanoff, Critical behavior. Universality and scaling, in *From Order to Chaos: Essays: Critical, Chaotic and Otherwise* (World Scientific, Singapore, 1993), pp. 222–239.
[72] R. Lipowsky, Shape fluctuations and critical phenomena, in *Fundamental Problems in Statistical Mechanics VII: Proceedings of the Seventh International Summer School on Fundamental Problems in Statistical Mechanics, Altenburg, F.R. Germany, June 18–30, 1989*, edited by H. van Beijeren (North-Holland, Amsterdam, 1990), pp. 139–170.